Journal Pre-proof

Pressure induced by roll-down foam-earplugs on earcanal

Ahmed S. Dalaq , Luiz G.C. Melo , Franck Sgard , Olivier Doutres , Eric Wagnac

PII: S0020-7403(22)00848-7
DOI: https://doi.org/10.1016/j.ijmecsci.2022.107970
Reference: MS 107970

To appear in: *International Journal of Mechanical Sciences*

Received date: 31 May 2022
Revised date: 22 November 2022
Accepted date: 22 November 2022

Please cite this article as: Ahmed S. Dalaq , Luiz G.C. Melo , Franck Sgard , Olivier Doutres , Eric Wagnac , Pressure induced by roll-down foam-earplugs on earcanal, *International Journal of Mechanical Sciences* (2022), doi: https://doi.org/10.1016/j.ijmecsci.2022.107970

Pressure induced by roll-down foam-earplugs on earcanal

Ahmed S. Dalaq[a,b,*], Luiz G. C. Melo[a], Franck Sgard[a,b], Olivier Doutres[b] and Eric Wagnac[b,c]

a: Institut de Recherche Robert-Sauvé en Santé et en Sécurité du Travail (IRSST), Canada

b: Department of Mechanical Engineering, École de technologie supérieure (ÉTS), Canada

c: Research center, Hôpital du Sacré-Coeur de Montréal (HSCM), Canada

Highlights

- Physical discomfort induced by earplugs is a persisting complain in surveys generated by labour worldwide.
- Physical discomfort is induced by mechanical stresses which can be treated via rigorous tribological models axisymmetric models.
- A J-Crimp machine that is typically used for stent characterization is used to assess the radial pressures induced by earplug on earcanal walls.
- Calibration of hyperelastic properties of skin and foam can generate representative pressure maps and displacement field across earcanal.

Abstract

Physical discomfort of earplug is a common complaint, so much so it jeopardizes the health and safety of workers, resulting in frequent noncompliance to proper wearing of earplugs. A pressing need thus arises to understand the underlying mechanics for the interaction of earplugs with earcanal walls. An idealized cylindrical geometry of earcanal is first treated with computational and analytical modeling to predict the pressure induced by roll-down cylindrical PVC foam earplugs. In order to predict representative pressure values and distribution, we estimated the hyperelastic properties of foam-based earplugs and characterized their behavior using a stent

Authors' accepted manuscript.
Article published in *International Journal of Mechanical Sciences*, Volume 241, 1 March 2023, 107970.
Version of record available at https://doi.org/10.1016/j.ijmecsci.2022.107970

testing machine (J-Crimp^{TM} machine) that mimics the radial compression of earplugs inside earcanals. Similarly, we estimated the hyperelastic properties of skin based on a simplified system consisting of a single hyperelastic layer. As a crosscheck of those found properties and calibrated models, we validated them with literature and against a set of three experiments: (i) earplug expansion in a cylindrical holder, (ii) quasi-static uniaxial and (iii) transverse compression. We finally used those validated properties of foam and skin to compute the pressure magnitude and distribution in an axisymmetric representation of earcanal as well as in a 3D realistic earcanal reconstructed from MRI images of a human subject.

*corresponding author; email address: ahmed.dalaq@mail.mcgill.ca

Keywords if applicable

Earplugs, Static Pressure, Earcanal, Finite Element Modeling, Hyperelasticity, Skin

1. Introduction

Noise induced hearing loss is a worldwide health issue. According to the Bureau of labor statistics, 1 in 9 of all recorded diseases is related to noise-induced hearing loss (NIHL) [1] in the United States (US). In Suzhou (China), in the year 2001, the rate of NIHL induced diseases reached up to 43.4% in urban areas [2]. These alarming statistics can be partly attributed to the discomfort associated with wearing earplugs. This discomfort may lead workers to wear earplugs incorrectly or in worse cases not wear them at all [3–8] while the claimed hearing protection is only achieved when earplugs are worn properly and consistently [9–11]. Even if provided with earplugs, about 3% to as high as 74% of workers in the United states (depending on the type of work) subjected to high noise levels do not use earplugs properly [12–16]. Comfort as a construct has recently been divided into four basic dimensions: (i) physical, (ii) acoustical, (iii) functional and (iv) psychological [3,4]. In this work we focus on the physical dimension and the role of the static pressure induced by earplugs on earcanal. The physical dimension has not yet been investigated as thoroughly as acoustical ones [17–22] despite its prominence in the construct of comfort.

The subjective part of physical discomfort can be captured through surveys and carefully designed questionnaires [4,23–25]. A result of several of these administered surveys have highlighted that "pain" is a common feedback from workers [4,23–25]. A strong component of the physical

dimension is the role of mechanical pressures and friction induced by earplugs on earcanal walls. Those indicators are objective quantities that can be found using rigorous methods of mechanics of materials. That in turn can contribute in developing objective comfort index for earplugs. Such an index is already present in various contexts as in for example the thermal comfort [26], computer wearables [27], manual saws [8], armchairs [28] , wheelchairs [29] and earmuff [30], but nevertheless absent for earplugs.

To the author's knowledge, studies on the mechanically induced pressure by earplugs on the earcanal are scarce [31–35]. One of the first studies on this topic was carried out in 1982, where the expansion force of earplugs was reported for 5 prominent earplug types using an experimental testing bench composed of two-pieces cylindrical sample holders (Supplementary materials 4, Figure S4a) [34,36]. Such an approach led to the evaluation of various earplugs in terms of earplug-induced expansion force which ranged between 1-3 N. The resulting mechanical load induced by earplug is generally referred to as static stress, equilibrium pressure or final expansion pressure. Throughout the manuscript, we denote it as static pressure, while the term "static" indicates that it is the pressure at steady state after full expansion of the earplug inside the earcanal when quasi-static condition applies. This static pressure is therefore mainly dependent on the hyperelastic material properties of the foam earplug, the skin, the geometric shape of the earcanal and the earplug. Knowing those information, simple idealized geometries can be treated with analytical methods. More complex geometric representations of earcanal are dealt with numerical methods such as using finite element (FE) models for predicting the static pressure [32,37]. A three-dimensional (3D) FE model was developed to model the interaction of an earplug with a 3D scanned human earcanal. They reported stress contours for three different earplugs under linear elastic setting for a rubbery earplug and earcanal [32]. This assumption of linear elastic material may be a reasonable simplification for skin because of the very small deformations experienced by skin, but a rough one for earplugs. Even so, earplugs that are stiffer than skin can still induce large deformations in skin, which further undermines the simple linear elastic assumption. Moreover, final shape of the earcanal and the earplug inside the earcanal depend on the relative stiffness of earplugs to that of earcanal. As such, soft earplugs may simply take the shape of earcanal, while stiffer earplugs, for example push-to-fit earplugs, may excessively deform the earcanal [38]. Another study utilized earcanal medical images to infer mechanical stresses through inverse calculation based on measured deformation of MRI scans [33]. Besides scarcity of works

in this domain, those investigations lacked experimental validation or verification with simple analytical models. Accordingly, a clear understanding of the mechanical interaction of earplugs with an earcanal is absent.

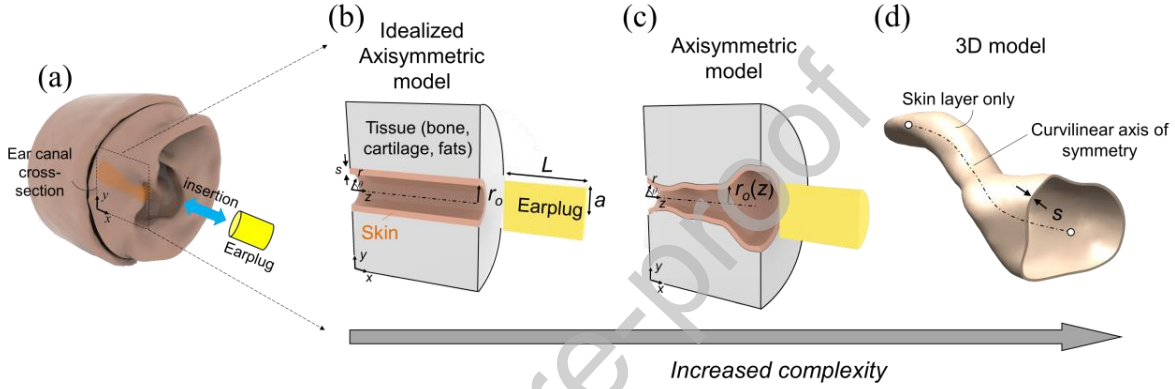

Figure 1. Earcanal modeling with progressive increase in model fidelity as depicted by a grey arrow at the bottom. (a) Actual curved earcanal profile cross-section (shown on *x*-*y* plane) is idealized into two axisymmetric models, where insertion direction of earplug is indicated as double sided blue arrow: (b) a simple straight cylindrical earcanal walls (i.e. earcanal radius of r_o = constant), (c) a more representative earcanal profile of that of actual earcanal walls where r_o varies along its axis *z*-direction. (d) Actual earcanal geometry. In (b), *s* is the skin thickness and *L* and *a* are axial length (along *z*-direction) and radius of earplug respectively.

To address abovementioned gaps in the literature, we convert actual 3D reconstruction of earcanal (Figure 1a) into three tribological models of increased model fidelity (Figure 1b,c,d). At first, we propose here a simple tribological model as an idealization of an actual 3D earcanal geometry (Figure 1a and 1b). This simple model consists of a cylindrical earcanal comprising a hyperelastic skin [39] interacting with a hyperelastic cylindrical roll-down (RD) foam earplug [40] lined with a linear-elastic bony/cartilaginous/fatty region [41,42] (Figure 1b). Mechanical analysis using the FE method and the simple analytical formulations of this axisymmetric system can be used to capture the underlying mechanics for the interaction of cylindrical RD-foam earplugs with

earcanal walls. This work will focus on the cylindrical 3M Classic™ polyvinyl chloride (PVC) RD-foam earplugs [43–45] because they are commonly used in noisy workplaces. We will refer to this type of earplug as RD-foam earplugs for brevity throughout this manuscript.

To the authors' knowledge, although several studies have provided hyperelastic properties of various polymeric foams [46–48], very limited data for RD-foam earplugs have been reported in the literature. Only elastic and viscoelastic RD-foam properties have been determined using static and dynamic uniaxial and transverse compression experimental tests [36]. To achieve sound and reliable prediction from these models, we use experiments based on J-Crimp [49] stent testing along with an FE-model of the associated RD-foam earplug. We will use the FE-model to simulate quasi-static compression to estimate the representative hyperelastic properties of RD-foam earplugs through optimization schemes [50]. For brevity, we refer to the quasi-static compression of earplug using the FE modeling as the "FE-model" throughout the manuscript. Similarly, we estimate the hyperelastic properties of skin using indentation experiments [39]. Next, we validate the FE-model of the RD-foam earplug based on the calibrated hyperelastic properties against experimental data from three different setups namely: (i) an expansion test of earplugs in a two-piece rigid cylindrical holder; (ii) quasi-static uniaxial compression measurements of cylindrical RD-foam earplugs from literature and (iii) transverse compression measurements of cylindrical RD-foam earplugs from literature. Finally, we extend the use of the validated FE-model and its hyperelastic properties to simulate the static pressure spatial distribution induced by an RD-foam earplug on both an axisymmetric (see Figure 1c) and 3D (Figure 1d) versions of a more realistic earcanal reconstructed from MRI images of a human subject.

2. Finite element modeling of a RD-earplug inside a cylindrical earcanal

Here we present a simple axisymmetric FE-model of an idealized case depicted on Figure 2a which simulates the interaction of a RD-foam earplugs with an earcanal. More specifically, we are interested in capturing the pressure magnitude and spatial distribution induced by earplugs on earcanal walls knowing mainly the material properties of earplug, skin and their effective diameters. The configuration of interest consists of an earplug with length L and radius a and earcanal with length H and radius r_o. Typically, earplugs are positioned between the first and second bend of earcanal surrounded by a mix of bony, cartilaginous and fatty tissues [51]. We idealize our model here into a skin layer with thickness, s and a bony/cartilaginous/fatty part

backing the skin with thickness B. Experiments showed that RD-foam earplugs induce insignificant earcanal deformation corresponding to a mean displacement <0.4 mm [38]. The surrounding tissue is therefore considered as elastic homogeneous materials with equivalent elastic properties much harder than skin or earplug (indicated as a hard substrate on Figure 2b). Thereby the earplug insertion depth in the idealized earcanal can be set arbitrarily as $0.13H$ because the material is homogeneous, where variations in the insertion depth has no effect.

The earplug adopted here is a large-size earplug with length of L=19 mm and diameter of $2a$=13 mm. Human earcanal radii commonly range between 3 and 4.5 mm [52], so initially we simulate and report results for r_o=3.5 mm, which leads to r_o/a=0.54. Similarly, H is chosen to be 30 mm since the earcanal lengths vary between 20 and 30 mm [52] . Skin thickness is s=1 mm [53]. The bony/cartilaginous/fatty part thickness is set arbitrarily to B= 6.6 mm.

Figure 2b shows meshed parts (i.e. earplug, skin and hard substrate) along the contact interaction between skin and earplug (designated in red). Parts are meshed with 3-noded triangular solid axisymmetric elements with linear shape functions (see Supplementary materials 1). The contact interaction between the skin and the earplug is enforced via Augmented Lagrange method for normal contact and penalty method for tangential contact interaction. Mesh refinement is applied inside the skin layer until the radial stresses are mesh-independent (Supplementary materials, Figure S1c).

To simulate the occlusion of the earplug into the earcanal while being compressed and its subsequent expansion in the earcanal, we divided the loading conditions into three steps (Supplementary materials 1, Figure S2). The earplug is constrained such that axisymmetric conditions are enforced (Figure 2b). The bony/cartilaginous part is considered fused with the skull and thus is subjected to fixed boundary conditions (Figure 2b and Supplementary materials 1, Eq. (S2)). This boundary value problem is solved with Abaqus solver [54]. We refined the mesh until pressure values and stress fields are converged and is mesh-independent (Supplementary materials, Figure S1c).

The skin is modeled as an isotropic solid with Neo-Hookean [43,45] constitutive law which has two parameters: shear modulus C_1 and bulk modulus K (see the orange box on Figure 2a). The associated strain energy density W is written as:

$$W = C_1(\lambda_1 + \lambda_2 + \lambda_3 - 3) + \frac{1}{2}K(J-1)^2 \quad (1)$$

where λ_1, λ_2 and λ_3 are principal stretches along 1, 2 and 3 respectively. $J = \lambda_1\lambda_2\lambda_3$, whereas the second term: $\frac{1}{2}K(J-1)^2$ determines the compressibility of the material, if the material is incompressible, the stretches satisfy: $J = 1$ which leads to $W = C_1(\lambda_1 + \lambda_2 + \lambda_3 - 3)$. The typical Neo-Hookean parameters of skin at room temperature range between 0.35−1220 kPa for C_1 and 0.014−63 MPa for K [39] whereas, cartilaginous, bony and fatty material possess typical properties of E =0.2−3 MPa [55], E=14−20 GPa [56] and 0.02 MPa [57] respectively. The hard substrate that represents the bony/cartilaginous/fatty region is modeled as a solid with a linear elastic constitutive law with two parameters: E=20 GPa, ν=0.3.

Typical Young's modulus of polymeric foam ranges between E=12−326 kPa [46–48]. The foam region can be modelled using Storaker's material model [40]. Storaker's model is governed by three independent parameters: shear modulus μ, and dimensionless empirical material constants α and β (see yellow box in Figure 2a). The strain energy density for Storaker's model is written as:

$$W = \frac{2\mu}{\alpha^2}\left[\lambda_1^{\alpha} + \lambda_2^{\alpha} + \lambda_3^{\alpha} - 3 + \frac{1}{\beta}\left(J^{-\alpha\beta} - 1\right)\right] \quad (2)$$

where μ is shear modulus, while α and β are hyperelastic material constants and J is the Jacobian. Typical hyperelastic polymeric foams properties of Polyurethane foam (PU-foam) as an example, are μ=6−163 kPa, α=2−55 and β=0.02−0.1 [46–48]. However, the earplugs of interest are made from a closed-cell PVC foam [36], having a density of 0.110 ± 0.002 g/cm^3, where ±0.002 is the standard deviation of the density variation over 10 samples. In addition, this type of foam has a thin crust on the external boundaries of earplug. Our preliminary uniaxial quasi-static compression test along the longitudinal axis of the earplug reveals a typical stress-strain ($\sigma - \varepsilon$) response of closed-cell polymeric foams, that is characterized with faint softening, no plateau regime (no prolonged zero-stiffness), and rapid densification at $\varepsilon \sim 0.8$. We also found that the Young's modulus along the longitudinal axis is about 35 kPa corresponding to a shear modulus $\mu \approx E/2 = 17.5$ kPa which falls within the abovementioned shear modulus range (See

Supplementary materials 6). PVC foam in general has an effective Poisson's ratios that range between ν = 0.09−0.23 (See Ref. [58,59]) which corresponds to β=0.08−0.16 (using Eq. (S7) in Supplementary materials 2). Our initial simulations using the model shown on Figure 2a and b, revealed that the forces and pressures within the model scale linearly with the shear modulus of the foam μ. We therefore normalized the foam shear modulus μ with that of the skin $2C_1$ as $\frac{\mu}{2C_1}$. This ratio is to be used throughout the manuscript. The above material properties lead to the range of $\frac{\mu}{2C_1} = 0.002 - 232$.

To develop a basic understanding of the interaction between skin and foam earplug we have adopted: μ=131 kPa, $2C_1$=72 kPa which leads to $\frac{\mu}{2C_1}$=1.8, which is within the range of abovementioned literature values. In addition, the foam earplug material was assigned typical nondimensional parameters of α=13.1, β=0.02 [46–48]. Section 4 and 6 focus on the estimation of earplug foam and skin actual properties respectively that will be used later in the manuscript for simulating representative 2D and 3D cases of earplug expansion inside the earcanal.

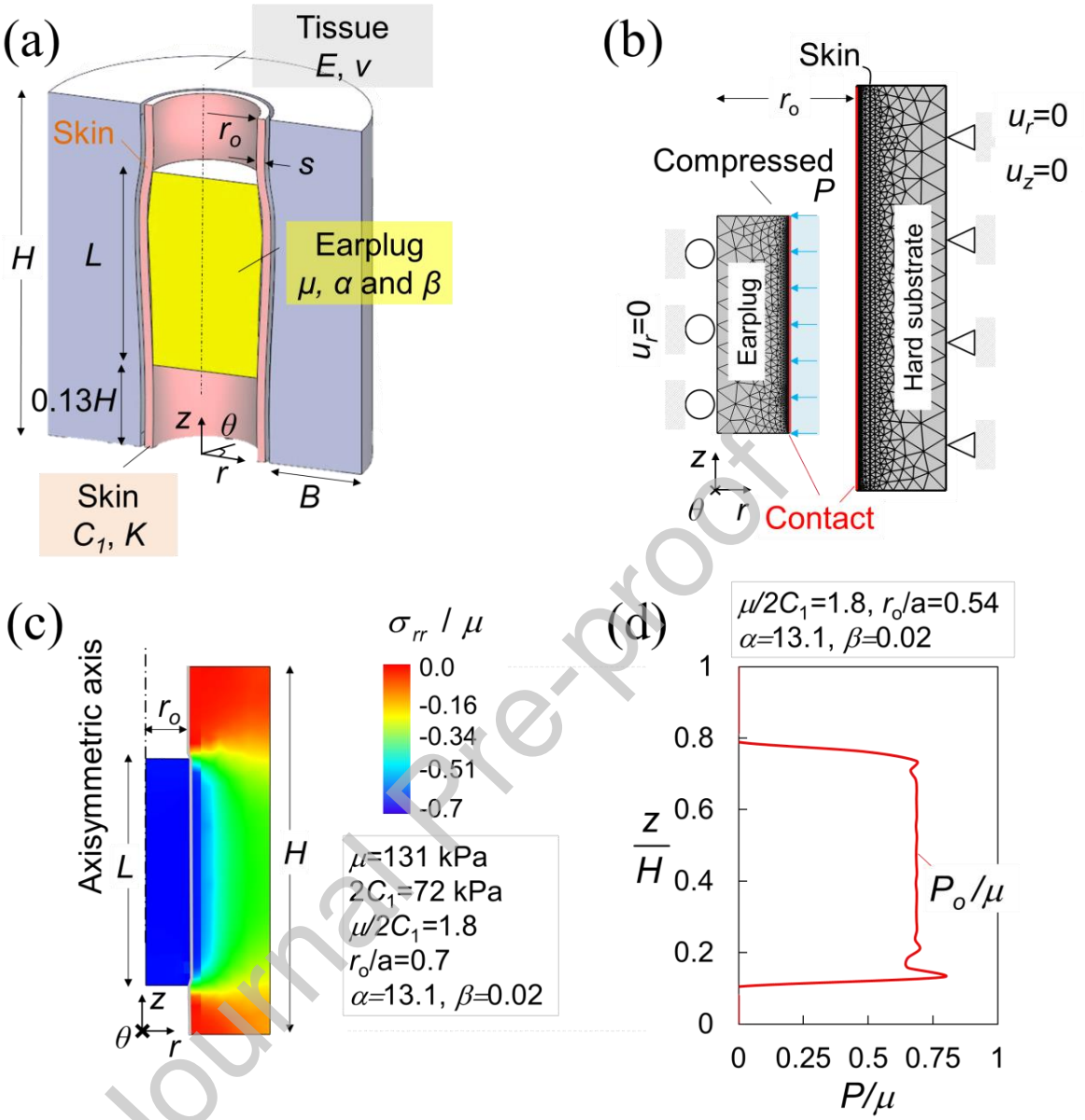

Figure 2. Axisymmetric FE-model and results: (a) idealized cylindrical earcanal occluded with earplug, (b) meshed FE-model, (c) normalized radial stress field distribution, (d) normalized spatial pressure distribution along earcanal walls.

Figure 2c shows the spatial distribution of normalized radial stresses field $\frac{\sigma_{rr}}{\mu}$ (Cauchy stress) inside earplug, skin and hard-substrate parts. Stresses inside earplug before and after making

contact with skin is constant and is simply $\sigma_{rr} = -P_o$ (see Eq. (S10a) in Supplementary materials 2). Because of the expansion of the earplug inside the earcanal once the radial loading P is released, the skin is subjected to compression with magnitudes that depend on μ and C_1. In turn pressure P_o is developed at the surface of skin. We are more specifically interested in the long-term value of P_o when the earplug has had time to fully expand. In practice, our experiment (in section 6) revealed that full expansion for foam earplug is typically achieved in about ~300 seconds once it is released. As such, inertial effects and viscoelasticity can be ignored. For $\frac{\mu}{2C_1}$=1.8, Figure 2d displays the normalized pressure distribution $\frac{P}{\mu}$ along earcanal wall. The absence of contact for $0 \le z/H \le 0.1$ and $0.8 < z/H \le 1$ leaves these boundaries with P_o=0 (i.e. free boundaries). For $0.1 \le z/H \le 0.8$ the earplug establishes contact and therefore pressure develops in this region. Small spikes in pressure at z/H=0.13 and 0.71 are attributed to the sharp corners of the earplug. These points of singularity (where theoretically $\sigma_{rr} \to \infty$ [60]) can be ignored and may not be of interest to analysis. Instead we focus on the middle region: $0.2 \le z/H \le 0.7$ where radial stress becomes $\frac{\sigma_{rr}}{\mu} = -\frac{P_o}{\mu}$.

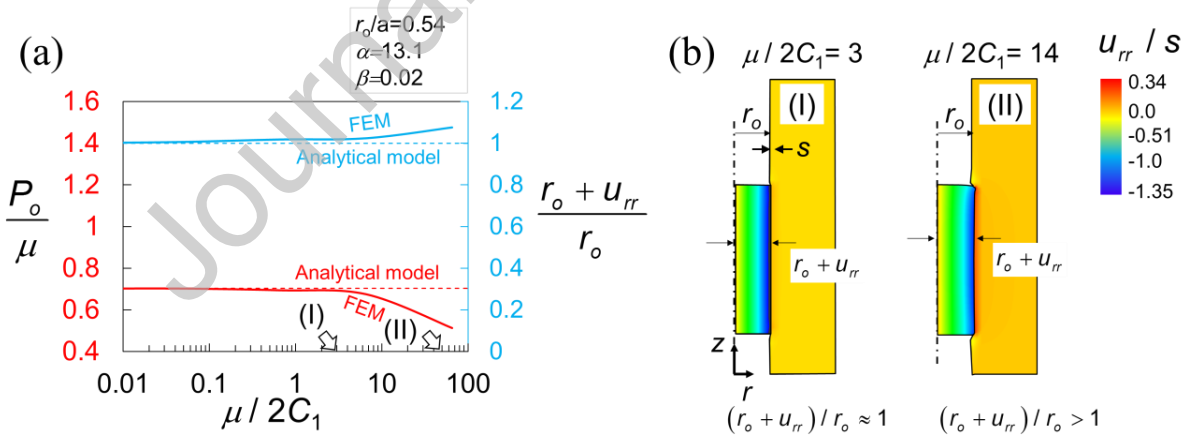

Figure 3. (a) Effect of relative softness of earplug foam to skin ratio: $\mu/2C_1$ on normalized contact pressure P_o/μ (in red) along with variation of normalized effective earcanal radius $(r_o+u_{rr})/r_o$ (in blue). (b) Radial displacement field demonstrating compressed earcanal walls for rigid (I) and soft skin (II) relative to earplug, respectively.

To assess the effect of the shear modulus of foam earplug μ and that of earcanal skin $2C_1$, we plotted the normalized contact pressure at earcanal walls $\frac{p_o}{\mu}$ as a function of $\frac{\mu}{2C_1}$ ratio (Figure 3a) along with their resulting radial displacement field normalized by skin thickness *s*: $\frac{u_{rr}}{s}$. We also show the $\frac{u_{rr}}{s}$ distribution for two examples cases: (I) and (II) at $\frac{\mu}{2C_1}$=3 and $\frac{\mu}{2C_1}$=14 respectively (Figure 3b). At low $\frac{\mu}{2C_1}$ (i.e. rigid skin), the earplug barely displaces the earcanal walls $r_o + u_{rr} \approx r_o$ (see case (I) on figure 3b). The blue curve on figure 3a shows that $\frac{r_o + u_{rr}}{r_o} \approx 1$ for low $\frac{\mu}{2C_1}$ ratios. The resulting pressure is constant P_o for $0 < \frac{\mu}{2C_1} < 7$ (red solid curve on figure 3a).

As $\mu/2C_1$ increases beyond $\frac{\mu}{2C_1}$>7, in other words as the skin becomes increasingly softer than earplug foam, P_o decreases. This corresponds to an increase in the final earcanal radius $r_o + u_{rr}$ due to excessive compression (displacement u_{rr} becomes >> 0) which leads to an increase in $\frac{r_o + u_{rr}}{r_o}$ (Figure 3a). This increase in final radius indicates that the earplug expanded slightly further by a displacement of u_{rr}. Figure 3b shows how the skin is undergoing excessive compression for $\frac{\mu}{2C_1}$=14.

3. An idealized analytical model for predicting static pressure induced by earplugs

The above results of the cylindrical tribological FE model indicate that P_o is sensitive to changes in the final radius $r_o + u_{rr}$ for $\frac{\mu}{2C_1}$>7. In addition, for $0 < \frac{\mu}{2C_1} < 7$, P_o is almost constant and independent of variation in $\frac{\mu}{2C_1}$. This finding suggests that assuming rigid skin relative to earplugs

($C_1 \to \infty$, $\frac{\mu}{2C_1}=0$ or a hard substrate for the surrounding material) in this range of values may actually be a reasonable assumption for RD-foam earplug-induced pressure prediction. These observations motivate the formulation of a simplified analytical model for the pressure distribution on earcanal walls that is induced by a soft earplug radially compressed in a "rigid" cylinder. Such model can be a handy alternative to the FE-model that represents the above tribological model for $0 < \frac{\mu}{2C_1} < 7$. The following analytical model will therefore assume $r_o + u_{rr} \approx r_o$ or $u_{rr}=0$ and a rigid skin where $\frac{\mu}{2C_1}=0$. Like the previously shown FE-model, earplugs are modeled as axisymmetric cylinders. As such, a point in the earplug is described by its cylindrical coordinates radius *r*, angle θ and height *z*. To find the radial static pressure induced by earplugs $\sigma_{rr} = -P_o$, we consider the earplug as a hyperelastic system, subjected to axisymmetric and equilibrium conditions [61] (see Supplementary materials 2, Eq. (S10)).

We assume a perfect radial compression, in which the outer surface of the earplug is compressed radially while maintaining the original axis of revolution, a point centroid and a circular outer surface at each state of compression. As such, the compression process can be represented as a kinematic mapping from reference frame $\{R, \Theta, Z\} = \{a, \Theta, L\}$ to current frame: $\{r, \theta, z\} = \{a_f, \theta, L_f\}$ (see Figure 4a) where the subscript *f* denotes "final" deformed configuration.

To relate the resulting deformation (stretches) with stresses, Eq. (2) that is the Hill and Storåker's hyperelastic strain energy density *W* is used [40]. Recall that *J* given by: $J = \lambda_1\lambda_2\lambda_3$, where λ_1, λ_2 and λ_3 principal stretches in *r*, θ and *z* directions respectively. The term $\frac{1}{\beta}\left(J^{-\alpha\beta}-1\right)$ accounts for high compressibility, a typical attribute of hyperelastic foams. $\beta \to 0$ represents a highly compressible foam, while $\beta \to \infty$ represents an incompressible foam. The Cauchy stresses are obtained by differentiating Eq. (2) [40] (Supplementary materials 2, Eq. (S8)):

$$\sigma_1 = \sigma_2 = \sigma_{rr} = \sigma_{\theta\theta} = \frac{2\mu}{\alpha}\frac{1}{J}\left(\lambda_1^{\alpha} - J^{-\alpha\beta}\right) = \frac{2\mu}{\alpha}\frac{1}{J}\left(\lambda_2^{\alpha} - J^{-\alpha\beta}\right) \tag{3a}$$

$$\sigma_3 = \sigma_{zz} = \frac{2\mu}{\alpha}\frac{1}{J}\left(\lambda_3^{\alpha} - J^{-\alpha\beta}\right) = 0 \tag{3b}$$

Solving (3a) and (3b) for the principal stretches we get:

$$\lambda_1 = \lambda_2 \tag{4a}$$

$$\lambda_3 = \lambda_2^{\frac{-2\beta}{1+\beta}} \tag{4b}$$

By definitions, principal stretches are simply the length in the deformed configuration divided by that in the initial one. For example, $\lambda_1 = \lambda_2 = a_f / a$ where a_f is the radius in the final configuration, therefore $\lambda_1 < 1$ because the earplug is under compression (Figure 4a). At equilibrium and after full expansion of the earplug, $a_f = r_o$, therefore $\lambda_2 = \frac{r_o}{a}$. Substituting Eq. (4a) and (4b) into (3a), we write σ_{rr} which is the pressure P_o induced by earplug at a known earcanal radius r_o as:

$$\frac{P_o}{\mu} = -\frac{2}{\alpha}\left(\left(\frac{r_o}{a}\right)^{\alpha-\frac{2}{1+\beta}} - \left(\frac{r_o}{a}\right)^{-2\left(\frac{\alpha\beta+1}{1+\beta}\right)}\right) \tag{5}$$

Equation (5) leads to a positive value of pressure, that is essentially a compressive stress: $\sigma_{rr} < 0$. Equation (5) also indicates that pressure P_o is directly proportional to the shear modulus μ. Figure 4b plots and shows the nonlinear relationship of $\frac{P_o}{\mu}$ with $\frac{r_o}{a}$. A smaller earcanal radius relative to earplug radius $\frac{r_o}{a}$ results in a larger P_o. For example, for α=13.1 and β=0.02, the pressure is $\frac{P_o}{\mu}$ =6, 1 and 0 for $\frac{r_o}{a}$=0.2, 0.4 and 1 respectively, whereas for $\frac{r_o}{a}$=0, the pressure is $P_o \to \infty$. As such, and according to Eq (5), different sets of (α, β) result in distinct normalized pressures $\frac{P_o}{\mu}$.

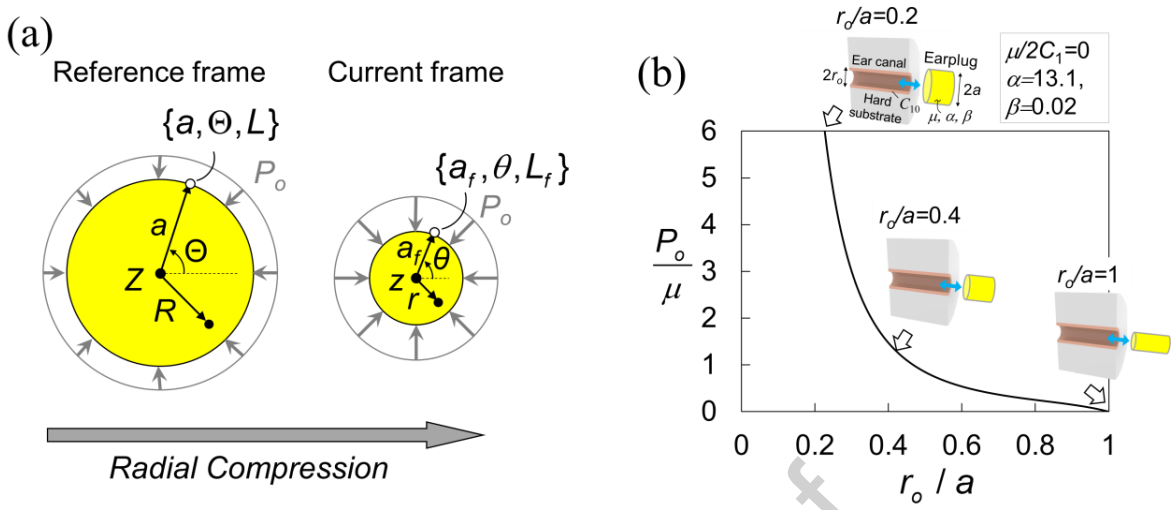

Figure 4: Analytical modeling of earplug compression. (a) Radial compression of earplug under radial pressure P_o. (b) Normalized radial pressure P_o/μ variation with normalized earcanal radius r_o/a.

For verification of Eq. (5), Figure 5a compares the FE predictions of normalized radial pressure $\frac{P_o}{\mu}$ for $\frac{r_o}{a}$ = [0.2, 1] (with steps of 0.1) for a rigid skin ($\frac{\mu}{2C_1}$=0) with the analytical model. The analytical model (in black) clearly captures the FE results (in red) quite well. Similarly, both FE- and analytical-models result in identical pressure values and profile along the earcanal walls for $\frac{r_o}{a}$=0.54 (Figure 5b).

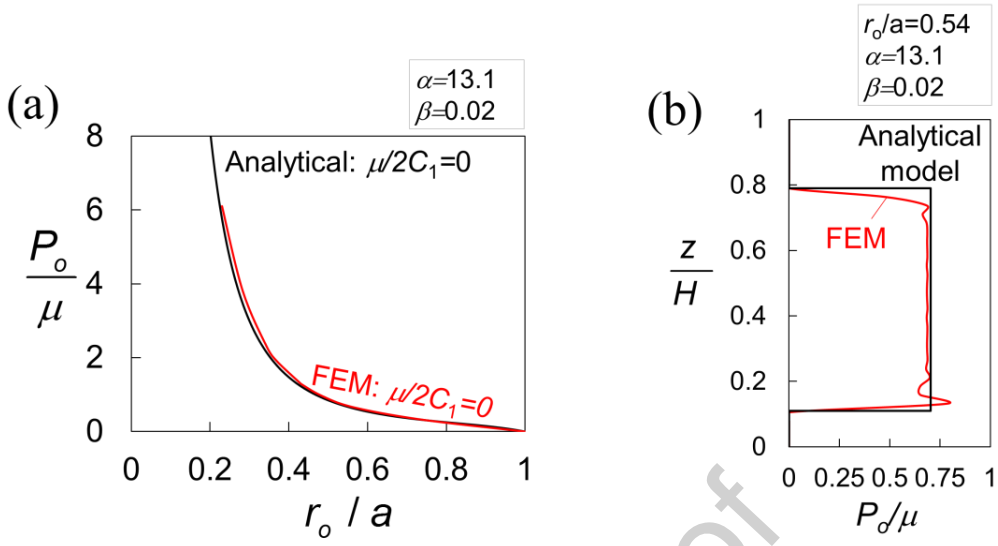

Figure 5: Verification of (a) radial pressure variation with earcanal radius r_o/a, (b) pressure distribution along earcanal walls of FE-model with analytical model.

Above sections showed how the mechanical interaction of a RD-foam earplug with the earcanal skin and magnitudes of P_o are dependent on the material properties of the earplug (μ, α, β) and skin (C_1, K). It is therefore needed to estimate the representative properties of earplug foam and skin as well as their relative shear modulus ratio $\frac{\mu}{2C_1}$. Those properties will also make it possible to evaluate the applicability of the proposed analytical model in light of Figure 3a.

4. Hyperelastic properties of RD-foam

In this section we estimate the hyperelastic properties of the foam (μ, α and β) from which the commercial RD-foam earplugs [44] are made out from. RD-foam earplugs are subjected to radial compression experiments, which are typically the loading experienced by earplugs inside earcanals. Catheter stents are subjected to similar pressure loading and regularly tested under radial pressure using J-Crimp stations from Blockwise (Tempe, Arizona, USA). Here we use this J-Crimp machine: TTR2 with J-Crimp™ station [49] to apply radial displacement loading on RD-

earplug (Figure 6a). Its key specifications are: 0−16 mm diameter range, 0.00074 mm diameter resolution, 660 N radial force maximum, 0.006 N radial force resolution, and ±0.4 N radial force friction level. The accuracy in terms of radial displacement is within ±0.05 mm at 10 N. The accuracy on the radial force for the J-crimp model is ±0.5 N.

At first, humidity is set to 50% and the temperature of J-Crimp chamber is controlled at 37 ºC, which matches the temperature inside human earcanal. Through this J-Crimp machine we subject three fresh earplug at a time (never compressed or rolled down before the experiment) to displacement-controlled loading where radial force at the surface of the earplug is transmitted from crimp teeth to a calibrated load cell. An actuation arm mechanism guides and converts radial motion of the crimp to vertical linear motion [62]. Radial forces are related to the vertical linear displacement and measured force by energy conservation, which neglects, frictional forces between the crimp and the tested object. The crimp dies are made from hardened stainless, so they act as rigid parts. Accordingly, we measure the radial force F_R and compute the static pressure using [63]:

$$P_o = \frac{F_R}{2\pi r_o L_f} \tag{6}$$

where L_f is the earplug length in the "final" deformed configuration (Figure 1b). Experiments revealed that the earplug surface length L that is in contact with the crimp is unchanged ($L_f \approx L$). However, the earplug exhibits slight bulging at the front and back surfaces. Pressure P_o is assessed in the deformed state of earplug with different r_o and thus represents the Cauchy stress.

A fresh earplug of nominal diameter $2a$=13 mm and length L=19 mm which are typical dimensions of RD-foam large sized earplug [44] is inserted inside the cavity of crimp teeth (Figure 6a). Figure 6b shows one example of a displacement-controlled loading profile applied on the tested earplug. After inserting the fresh earplug, crimp teeth undergo a decreasing slow radial displacement at a rate of 0.15 mm/s until a desired diameter is reached: $2r_o$=4 mm (at $0 < t < 75$ s on Figure 6b). This diameter is maintained while the earplug undergoes full relaxation until t=450 s. For this particular loading profile (Figure 6b) and because of radial displacement, radial pressure rises exponentially

up to P = 226 kPa (see Figure 6c), and as soon as radial displacement stops at t=75 s, the force slowly decays leading to a steady state pressure P_o=100 kPa for t > 300 s (i.e. the static pressure). In terms of mechanics of materials, this measured static pressure is mechanically equivalent to the static pressure obtained from the analytical model and FE-model (P_o that of Figure 5a). In other words, the pressure resulting from quasi-static compression (very slow compression) of the earplug (e.g. Figure 4b) to a specific diameter $2r_o$ as simulated by the FE-model, is equivalent to steady state pressure P_o reached after relaxation to the same $2r_o$ performed in experiments. In both cases, dynamic and viscoelastic effects have eventually subsided. However, the exponential increase and decay in the initial part of the experimental curve ($0 \le t < 300$ s) are function of viscoelastic properties and so subject to strain rate effects. This initial part is ignored because the main objective of these experiments is to measure the static pressure P_o for various final diameters $2r_o$. We have repeated the above procedure for r_o/a=0.31, 0.469, 0.625, 0.718 and measured the corresponding steady state pressure P_o. Figure 6d shows the experimental variation of the raw P_o with r_o/a where the shaded area in light blue represents the variations of the three tested samples.

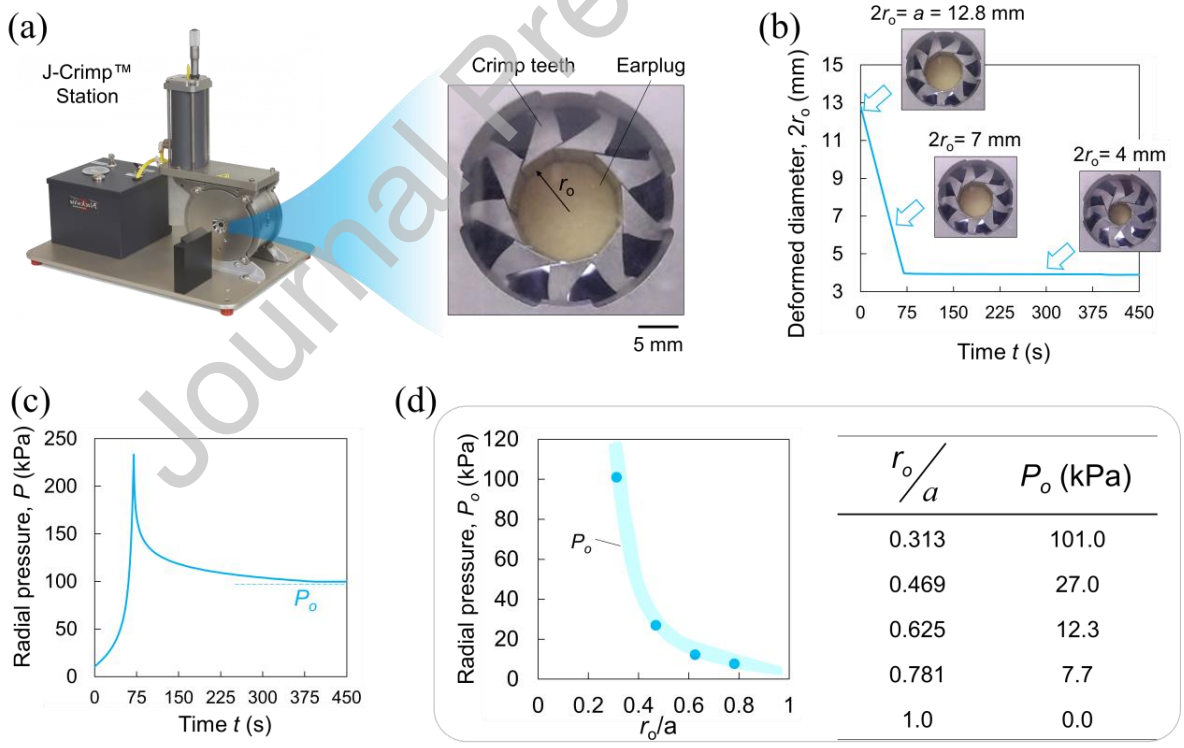

Figure 6: Experimental setup and procedure, (a) J-Crimp^{TM} Station with crimp teeth applying displacement-controlled load on an earplug (yellow cylinder), (b) an example of displacement-time profile, (c) the resulting pressure variation

with time: P_o–t curve. (d) Raw averaged value of pressure P_o data at different compression radius r_o along with their tabulated values shown to the right of the plot. J-Crimp picture is adapted from [49].

This raw experimental data can now be used to calibrate the FE-model (of section 2) by finding actual hyperelastic properties (μ, α and β) of the tested RD-foam earplug. Note that variable β mainly controls materials elongation, bulging and "barreling" of the foam, which are kinematic attributes that are ignored in this study. We rather focus on calibrating the foam properties for prediction of pressure. In addition, subjecting those earplugs to uniaxial compression reveals negligible "barreling" and thus minimal Poisson's effect (See Supplementary Video S1). We have therefore assumed the lowest value of β for PVC foams found in the literature, namely β = 0.08 and used the experiments to calibrate (μ, α).

In the calibration process, our objective is to minimize the residual error of the pressure prediction based on the FE model $P_o^{FE}(u_e)$ relative to experiment $P_o^{EXP}(u_e)$ which can be written as:

$$f(\mu,\alpha,\beta)=\sum_{e=1}^{n}\left(P_o^{FE}-P_o^{EXP}\right)^2 \tag{7}$$

where those pressures are computed at the experimental compression ratios $\frac{r_o}{a}$. Here we use four experimental data points (i.e. n=4) tabulated on Figure 6d.

An initial full factorial sweep over the 2D parameter space (μ, α) on a fixed plane of $\beta = 0.08$ revealed that the minimum of $f(\mu,\alpha)$ lied within the blue region $0.5\ \text{kPa} \le \mu \le 2\ \text{kPa}$ and $0 < \alpha \le 15$ (Figure 7a). Beyond this region the residual error spikes exceeding $f(\mu,\alpha) > 2000$. The minimum point can be determined by the minimization of Eq. (7) using Nelder-Mead Simplex Method optimization algorithm [50] subjected to constraints: $\mu \in [0,40]\ \text{kPa}$, $\alpha \in (0,50]$ and $\beta = 0.08$. These bounds were selected based on typical ranges of these properties obtained from previous studies [46–48] (see section 2). The lowest sums of residuals was $f(\mu,\alpha,\beta=0.08)=8.5$ that corresponds to a maximum error of 4.6% with respect to J-Crimp experiments. This minimum value is obtained at μ=11.4 kPa, α=8.57. These estimated hyperelastic properties also satisfy the stability criterion [45] and can therefore be used in other

computational works (Supplementary materials 3, Figure S3). In addition, as an additional crosscheck Figure 7b shows that the FE-model results computed for μ=11.4 kPa, α=8.57 and β=0.08 match the calibration experiments with error range of 2−4.6%.

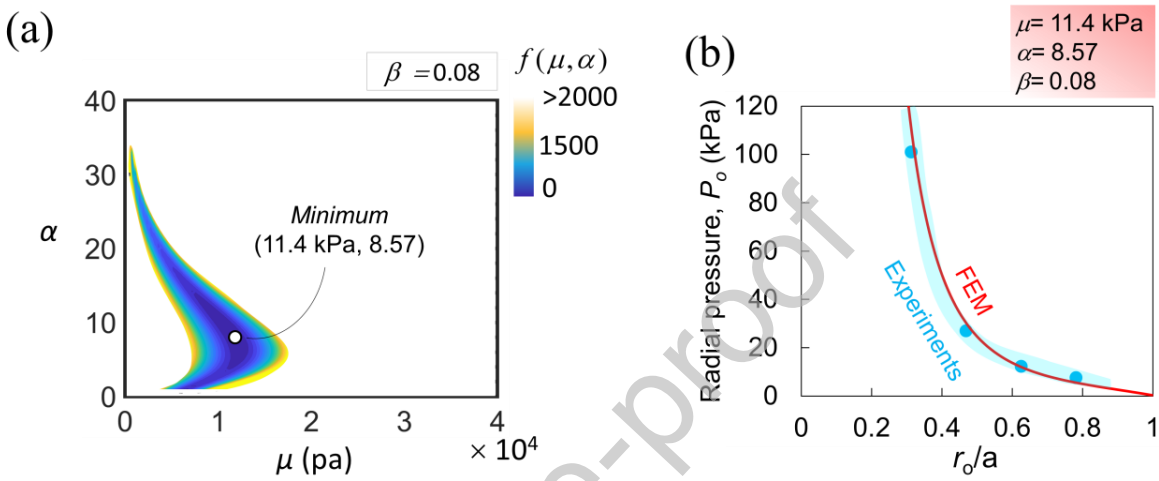

Figure 7: (a) Full factorial sweep over the material parameter space (μ, α, β = 0.08); (b) Verification of FE-model using the found hyperelastic properties of the earplug and its comparison with experiments.

5. Validation of the FE model of RD-foam

This section presents several experimental setups to validate the RD-foam earplug FE-model which has been calibrated with the hyperelastic properties determined in section 5. In the first setup, an experiment is performed by measuring the transverse force F_T generated by earplug during its expansion. Subscript T stands for transverse. The experimental setup consists of two disconnected conforming rigid parts, forming a cylindrical cavity of final diameter $2r_o$ that houses the earplug (Figure 8a). The upper sample holder is supported by a rigid flat plate at a fixed location (x, H) and is connected to a load cell to measure F_T while a fixed anvil at the bottom supports the lower conforming half. The load cell is a 100 N capacity Instron (2530±100N) series which is a resistive force transducer with 0.2% repeatability error.

Unlike the crimp test, here the earplug is first rolled down (i.e. pre-compressed radially by hand)

and then positioned inside the cavity. The earplug is left to expand until it establishes contact with the sample holder. The total transverse force measured during this process is plotted as a function of time on Figure 8b. Figure 8b shows the transverse expansion force F_T for $2a$=13 mm and $2r_o$=7 mm. The force keeps rising for 50 s and then stabilizing at around 150 s. We repeated this experiment for $2r_o$=7, 8.5 and 10 mm for the same type of earplug $2a$=13 mm using 4 fresh earplugs for each value of final diameter $2r_o$ (Figure 8c). The blue shaded area represents the maximum and minimum error margin of measured F_T values. Those RD-earplugs are sensitive to the amount of precompression, as we have observed qualitatively that with more precompression the final static pressure gets lower. This behavior can be attributed to damage incurred during the precompression. Therefore, the hand precompression contributes to variations in the experimental measurement.

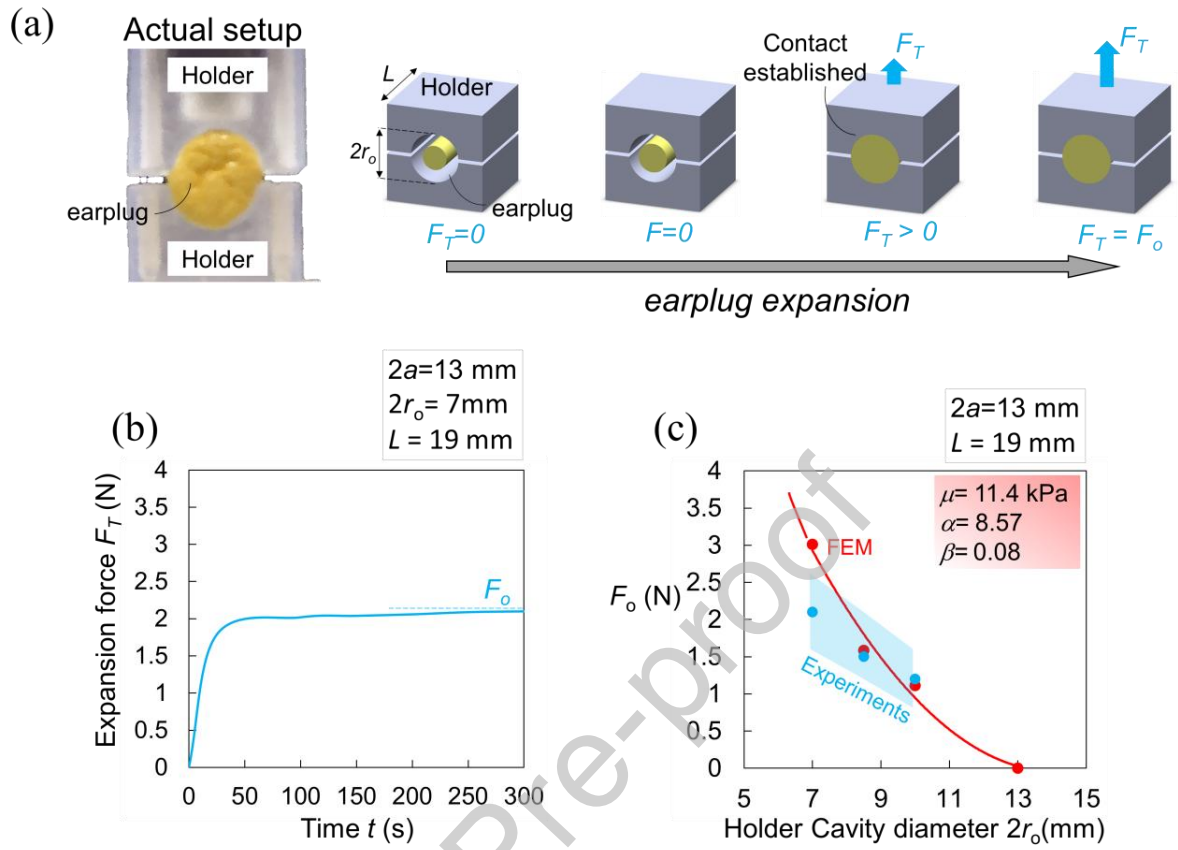

Figure 8: (a) Experimental procedure and stages of deformation from insertion of earplug inside the holder to full expansion; (b) Resulting experimental transverse expansion force with time: F_T–t; (c) evaluation of calibrated hyperelastic properties (section 4) used in FE-model in comparison with corresponding experimental data of expansion test.

Using an equivalent FE-model of this experiment with the previously found RD-foam hyperelastic parameters: μ=11.4 kPa, α=8.57 and β=0.08 (see details in Supplementary materials 4, Figure S4a), we calculate the transverse reaction force resulting from the expansion of the earplug until it reaches the final steady state force F_o. The calculated force F_T during expansion in the FE-model may not be relevant and/or comparable to the corresponding experimental data because viscoelastic and dynamics effects occurred in experiments in this time window. Instead, the parameter of interest here is F_o which is at steady state in experiment and which corresponds to that of the static FE-model (Figure 8b). Figure 8c compares the FE prediction of F_o with experiments. The solid red line is a best fit of simulated FE data points (in red circular markers). The FE–model calculations using the identified foam parameters match experiments (in blue

circular markers) reasonably, especially for large values of r_o. The discrepancies between FE results and mean experimental values (the round blue marker on Figure 8c) are 40%, 5.4% to 7.3% for $2r_o$=7, 8.5 and 10 mm respectively. Those large discrepancies between FE-model and experiments for small $2r_o$ = 7 mm (r_o /a=0.54) could be attributed to the presence of friction in experiments which is not accounted for in the simulations. This friction is also ignored in the radial force measured with Blockwise experimental setup [62]. Possible variation in the intrinsic earplug properties resulting from variations of manufacturing conditions, together with the effects of hand precompression, may have contributed to those errors, despite best efforts in ensuring repeatable precompression. In addition, during compression, the earplug surface may wrinkle so that the outer surface does not remain perfectly cylindrical (Figure 8a reveals some wrinkles). Differences in temperature and humidity levels between the calibrating setup shown on Figure 6a and that of the validation on Figure 8a may also contribute to the error.

The second validation of the RD-foam earplug of foam properties is accomplished by developing two additional FE-models that simulate the static-transverse and -uniaxial compression of RD-foam earplugs reported by Berger [36] (Supplementary materials 4, Figure S4b and c). In Berger's experiment, earplugs with dimensions $2a$=13.7 mm and L=20 mm [64] were allowed to expand between two plates in uniaxial and transverse directions at 60% of height and diameter respectively or, in other words, at stretches of $\lambda_T = \lambda_U = 0.6$, where subscripts T and U denote transverse and uniaxial respectively.

Using the foam parameters identified in section 4, we compute F_T using the FE model which is plotted as a function of stretch during compression in the left panel of Figure 9a (red solid line). The corresponding field displacement is shown for two stretches: $\lambda_T = 1$ (initial state) and $\lambda_T = 0.45$ in the right panel. Similarly, the compression force F_U is shown along with its corresponding displacement field u_y for $\lambda_T = 1$ and $\lambda_T = 0.2$ (Figure 9b). The results of Berger [36] are indicated in both plots as blue filled circular markers. To the right of those plots, the bar plot compares individual values of Berger's with FE-model prediction. For the transverse direction, which is the direction of interest for our application, the error is around ~2.5%, whereas along the uniaxial direction it is up to ~90%, which suggests that Berger's earplug may be anisotropic. However, the found hyperelastic properties (μ=11.4 kPa, α=8.57 and β=0.08) are capable of capturing the response along the direction of interest (i.e. along the radial directions and to large extent the

transverse one). Recall that our preliminary longitudinal compression of the earplug (see supplementary material 6) leads to a shear modulus of $\mu \approx 17.5$ kPa, that is 1.5 times higher than that along radial direction which suggests that those earplugs may actually be anisotropic. Anisotropy may have resulted from the cutting process of foam into cylinders and/or the presence of crusts on the boundaries of the earplug.

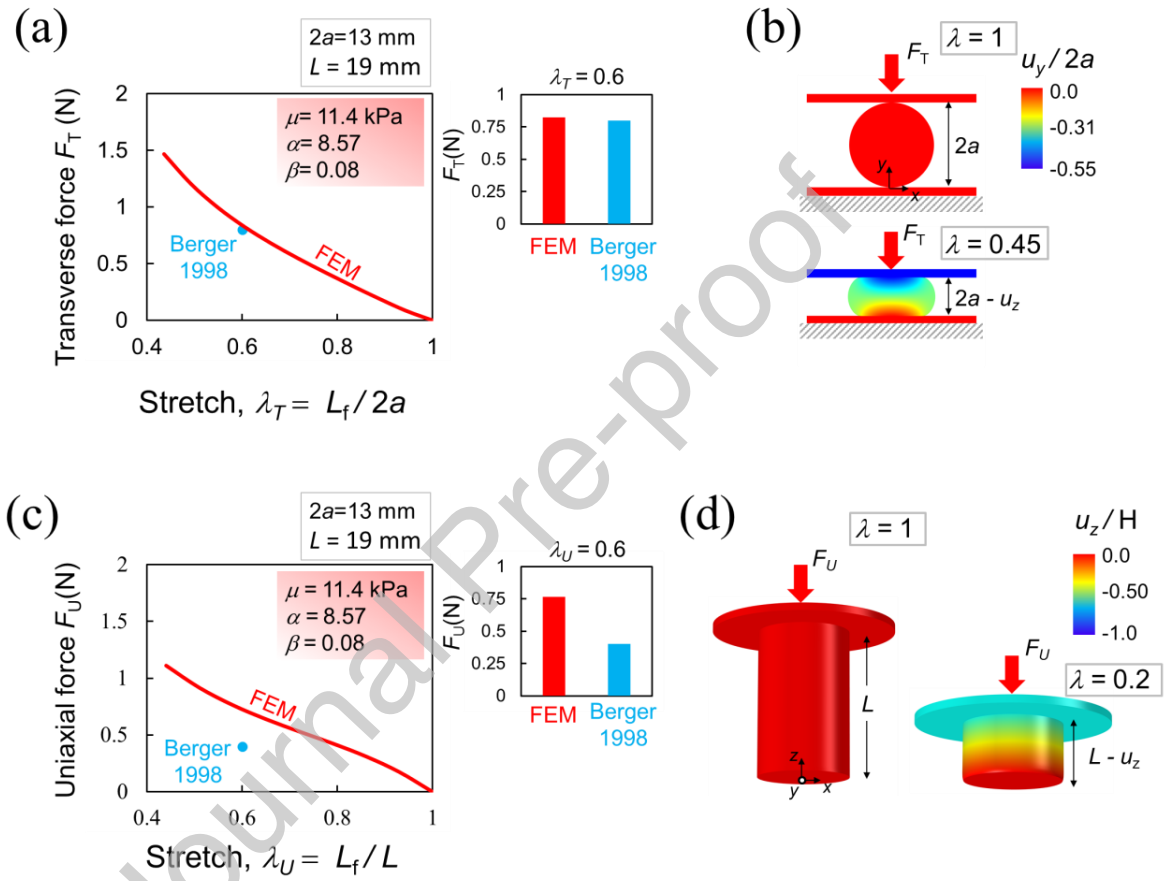

Figure 9: Comparison of the FE predictions with experiments from Ref.[36] for transverse and uniaxial quasi-static compression. (a) Transverse force and (b) corresponding normalized displacement field $u_y/2a$ (c) Compression force and (d) corresponding normalized displacement field u_z/H.

6. Hyperelastic properties of skin

In this section, we focus on the assessment of skin hyperelastic mechanical properties based on Tran et al 's [39] work. These authors performed indentation experiments on actual forearm via a cylindrical indenter. They estimated the hyperelastic properties of the skin based on a Neo-Hookean model through FE modeling of the three skin layers (epidermis, dermis, and hypodermis)

including the relatively soft muscle tissue. Therefore, in this paper we use those experimental data to determine the hyperelastic properties of earcanal skin assuming a simplified homogenous hyperelastic elastic block that is representative of skin (Figure 10a). The simulation dimension and the hyperelastic block match the indented forearm section of the experiments [39]. As such, our analysis assumes forearm skin as a representation of skin in earcanal. This assumption is reasonable in view of the similarity between forearm skin and earcanal ones [65]. The FE model simulates the actual experimental procedure for indentation with an indenter of radius to characteristic skin and forearm size ratio R/b=0.07 (R=2.64 mm, b=40 mm) (Figure 10a). We model this single layer using a Neo-Hookean model [66] with two hyperelastic properties: $2C_1$ (equivalent to shear modulus) and K (bulk modulus). The indenter represented by the circular domain at the top is subjected to a downward displacement of $-0.2b$:

$$u_y(b/2+R) = -0.2b \quad \text{at indenter's center} \tag{8a}$$

The bottom of the skin layer is fixed:

$$\begin{aligned} u_x(-b/2) &= 0 \\ u_y(-b/2) &= 0 \end{aligned} \tag{8b}$$

All remaining surfaces are free (i.e. traction $\mathbf{t} = 0$). This boundary value problem is solved using COMSOL Multiphysics [67]. During indentation, we calculate the reaction force F at the indenter (Figure 10a). Mesh is refined until F and field results (stresses and displacements) are mesh-independent. Figure 10a at the bottom (at $y= -b/2$) shows the vertical normalized displacement field u_y/b after indentation. The top surface of the skin ($y= +b/2$), takes a pitting curved shape upon indentation which is due to the soft hyperelastic response of the skin. During indentation, the FE-model can now generate a force displacement curves $F-u$ for any C_1 and K values. To identify C_1 and K, an objective function (or cost function) $f(C_1, K)$ measuring the overall residual error between the experiments of Tran et al [39] and our computed reaction force obtained for 6 different indentation displacement is defined as:

$$f(C_1,K) = \sum_{e=1}^{6} \left(F_{exp}(u_e) - F_{FE}(u_e) \right)^2 \tag{9}$$

Equation (9) is minimized using a brute force optimization procedure. In Eq. (9), $F_{\exp}(u_e)$ is the experimental reaction force at an indentation displacement u_e, while $F_{FE}(u_e)$ is the reaction force computed using the FE-model. The material parameters were varied with stepping increment of 5000 Pa in the ranges $C_1 = \left[500, 2\times10^5\right]$ Pa and $K = \left[5\times10^4, 8\times10^6\right]$ Pa, which we used to map the entire material, space of $f(C_1, K)$ within said bounds.

Figure 10b shows $f(C_1, K)$ map plotted in 2D space. The dark blue region indicates probable location of the minimum. To pinpoint that minimum, we use Nelder-Mead Simplex Method [50]. The optimization algorithm leads to $C_1 = 36$ kPa and *K*=1.14 MPa, where both values are within the range of previously mentioned literature data [39]. Using those hyperelastic parameters, the reaction force as a function of the indenter displacement is recalculated using FE-model. A good match between FE results and experiments [39] is obtained (Figure 10c). The values of $f(C_1, K)$ in the 2D design space shows relative insensitivity to changes in *K*, particularly in the vicinity of the minimum point. It is therefore reasonable to assume an incompressible model (i.e. *J*=1) for skin (Supplementary materials 1, Eq. (S1)).

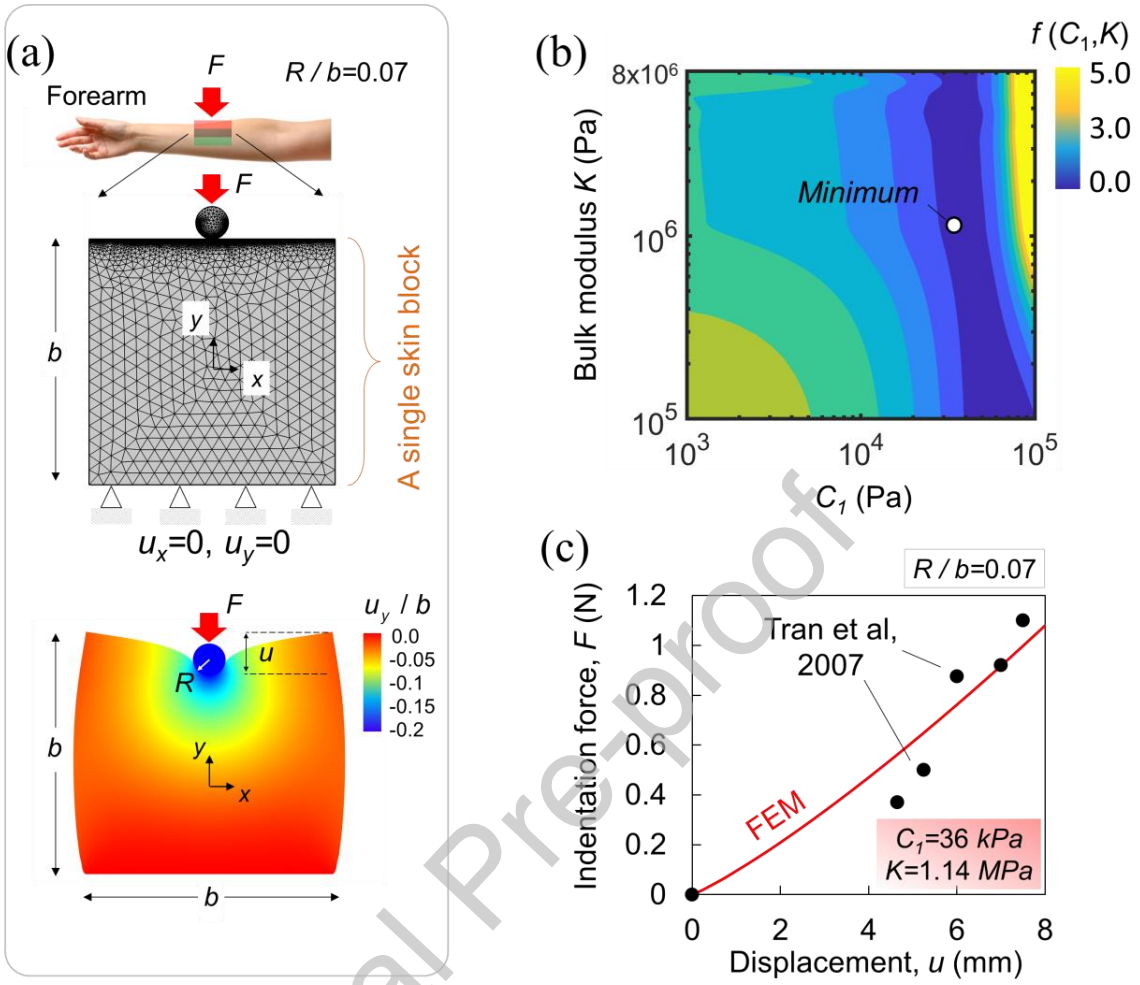

Figure 10: The three layers of skin: epidermis, dermis and subcutaneous are modeled as a single layer. (a) Meshed finite element model (FE-model) with boundary conditions representing a cylindrical indenter indenting a single layer of skin (top), the resulting normalized displacement field u_y/b contours (bottom). (b) log-log plot of objective function contour as function of K and C_1, with the minimum point (C_1=36 kPa, K=1.14 MPa) is denoted by a filled white circular marker. (c) Comparison of experiments of Tran et al [39] with FE simulations.

7. Pressure in a more realistic axisymmetric earcanal

In this section, we present FE simulations that account for actual curvatures of earcanal. To do so, we obtained a full 3D geometric model constructed from high-resolution MRI images based of a healthy human subject (a volunteer male participant of 29 year of age [38,51]) without any known hearing impairment or earcanal abnormalities. Figure 1a shows the CAD model constructed from those MRI images. This 3D model consists of the earcanal surface topology, part of the pinna as

well as the surrounding tissues (bone, cartilage and fats). We isolated the earcanal surface from the rest of the parts, which we converted it to its respective point cloud. Using this point cloud, we can either construct an axisymmetric representation (Figure 1c) of the earcanal surface or a realistic 3D model of earcanal (Figure 1d). The point cloud of the earcanal internal surface can be sliced into a set of representative cross sections made of circles and the locus of their centroids correspond to a curvilinear axis (dotted axis on Figure 1d). This curvilinear axis can be "unwrapped" along its arc length into a straight axis of symmetry to form an axisymmetric model. Earcanal entrance and eardrum act as references for marking the beginning and the end of the geometry respectively. The following subsections present FE modeling of axisymmetric and 3D earcanal model respectively.

7.1. Axisymmetric model. In this section, we predict the pressure induced by earplugs using the analytical model and FE model in the case where the RD-foam earplug is inserted in a more realistically shaped earcanal. We aimed first to build an axisymmetric model with varying cross-section areas along the earcanal axis. The FE-model is similar to that of the cylindrical earcanal namely identical boundary conditions and frictionless contact interaction but it differs by the profile (radius as a function of z). This profile is obtained from the 3D geometry by considering circular cross-sections of equivalent areas to the actual ones. The associated curved profile is shown in Figure 11a, where skin free surfaces are indicated in grey line while in-contact boundary is indicated in black.

The analytical model presented in section 3 is not limited to a constant r_o. Indeed, by substituting the varying $r_o(z)$ of this curved profile, or of any axisymmetric representation of earcanal in Eq. (5), we may have an estimate of the radial pressure at earcanal walls $P_o(z)$ that is now a function of z:

$$\frac{P_o(z)}{\mu} = -\frac{2}{\alpha}\left(\left(\frac{r_o(z)}{a}\right)^{\alpha-\frac{2}{1+\beta}} - \left(\frac{r_o(z)}{a}\right)^{-2\left(\frac{\alpha\beta+1}{1+\beta}\right)}\right) \tag{10}$$

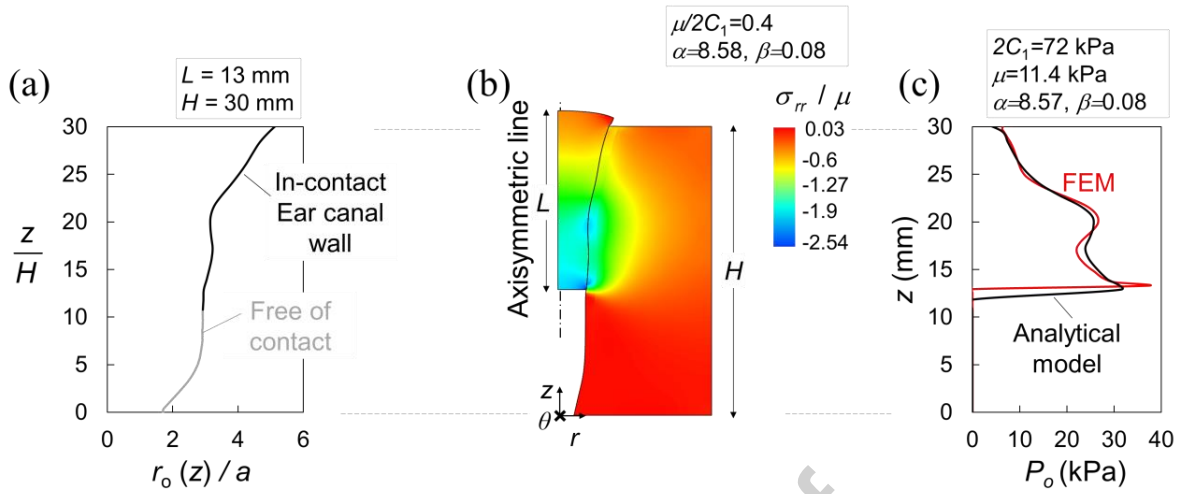

Figure 11: (a) Coordinates of the curved earcanal profile $r_o(z)$; (b) Radial stress field obtained from FE axisymmetric model and (c) earplug-induced pressure along the curved earcanal walls from FE-model (in red) and analytical models (in black).

Figure 11b shows the normalized radial stresses $\frac{\sigma_{rr}}{\mu}$ (Cauchy stresses) inside the earplug, skin layer and the hard substrate part of the FE-model for the calibrated foam and skin parameters: μ=11.4 kPa, α=8.57, β=0.08 and $2C_1$=72 kPa which gives $\frac{\mu}{2C_1}$=0.158. Unlike cylindrical earcanal, the stresses inside the earplug and at the interface between earplug and earcanal walls (at the skin) vary with both with r and z coordinates. Normalized stresses σ_{rr} and P_o along the earcanal wall computed using the FE-model are displayed on Figure 11c. Contact free surfaces of skin exhibit zero pressure, whereas the middle section: $11 \le z \le 30$ mm, is subjected to compression from the earplug and therefore shows finite variation in pressure P_o. The FE simulation interestingly reveals a variation in pressure consistent with variations in r_o. Narrower (small r_o) sections result in higher local magnitudes of pressure $P(r_o)$ and vice versa (recall P_o trend with r_o of Figure 5a). The resulting radial stress calculated using Eq. (10) is also plotted in Figure 11c. The analytical and the FE-models agree quite well. Based on this FE prediction, the RD-foam earplug subjects this earcanal to a varying pressure in the range of P_o=5−31 kPa.

7.2 Pressure in a 3D earcanal

In this section, we simulate the expansion of a RD foam earplug inside the 3D earcanal geometry. The 3D point cloud of the internal earcanal surface was meshed, patched and thickened by s=1 mm, which forms a skin layer (Figure 12a). Similar to previous section, the skin is modeled using the Neo-Hookean model with the set of representative properties found in section 4 and 5. In contrast, for simplicity and for computational efficiency, this thickened skin layer is not backed by a hard substrate. Instead, we simulate two extreme cases where the earcanal skin layer is backed by rigid materials or by an extremely compliant one. Those extreme cases are achieved by applying fixed boundary conditions or traction free surfaces on the outer boundary of the skin layer (Supplementary materials 5, Figure S5). The earplug is compressed to a diameter of 5 mm and inserted inside the earcanal cavity. The earplug is made parallel with y–x plane (see front view on Figure 12b) and its longitudinal axis is tilted by an angle of θ=18.8° with respect to the horizontal axis (x-axis) and its frontal center is 16.1 mm far from that of the eardrum (Figure 12a). The earplug is inserted such that that its position lies between the first and second bend, which is a typical position for a RD earplug [38].

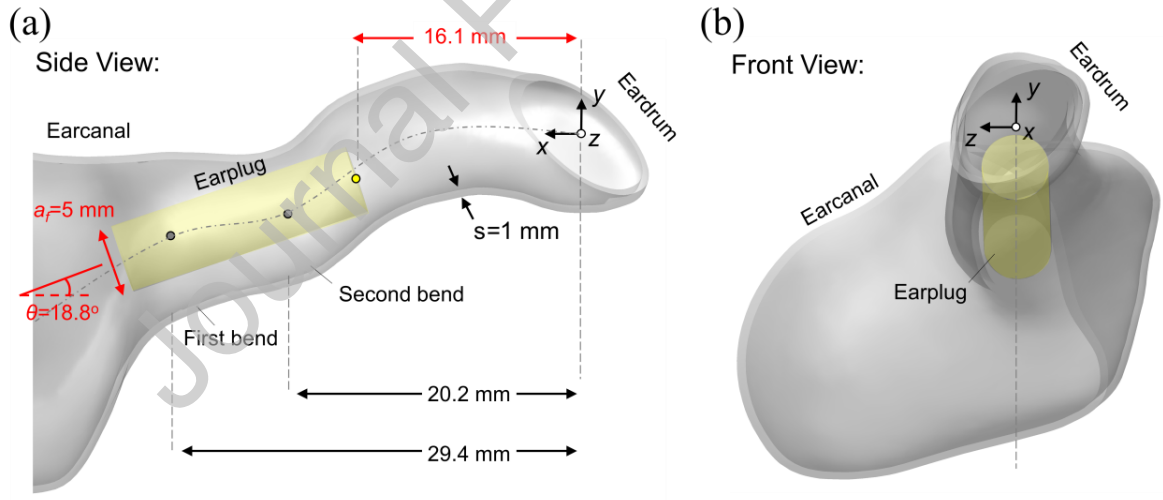

Figure 12: Actual earcanal geometry showing the relative position of the compressed earplug inside the earcanal in (a) Side view and (b) front view.

Figure 13a shows the pressure contour at the internal surface of the earcanal. Interestingly, the earplug takes the shape of the earcanal and the region of highest pressures stretching along the first and second bend ranges between 13−18.2 kPa. Figure 13b zooms on the earcanal regions of entrance, highlighting the high stress points and compares the pressure magnitudes of simulations (bare plots in red) with the estimates of the analytical model (bar plots in grey).

The highest stress points occur at radiuses relative to deformed longitudinal axis of the earplug of r_o=3.49, 3.26 and 4.75 mm, with pressure magnitudes of P_o= 18.2, 17.9 and 13 kPa respectively. At those radiuses, the analytical estimates pressures of 18.5, 9.8 and 6.7 kPa, respectively. Unexpectedly, the highest stress did not occur exactly at the minimum radius that is r_o=3.0 mm, but is still in the vicinity of the high stress region. That is the region confined between the first and second bend where the earplug is pinched and twisted. The discrepancy between analytical and 3D FE-model arises because axisymmetric conditions are not applicable anymore for the tortuous earcanal. Indeed, other stresses such as shear, bending and torsional stresses emerge. As such, high fidelity 3D models is essential for obtaining accurate predictions of pressure. The earcanal surface and earplug did not undergo displacement because of the prescribed fixed condition around the skin. The pressure displayed here are therefore considered as the upper pressure limit of what can be obtained for such an earplug (inserted in such an earcanal) because of this rigid confinement of the earcanal.

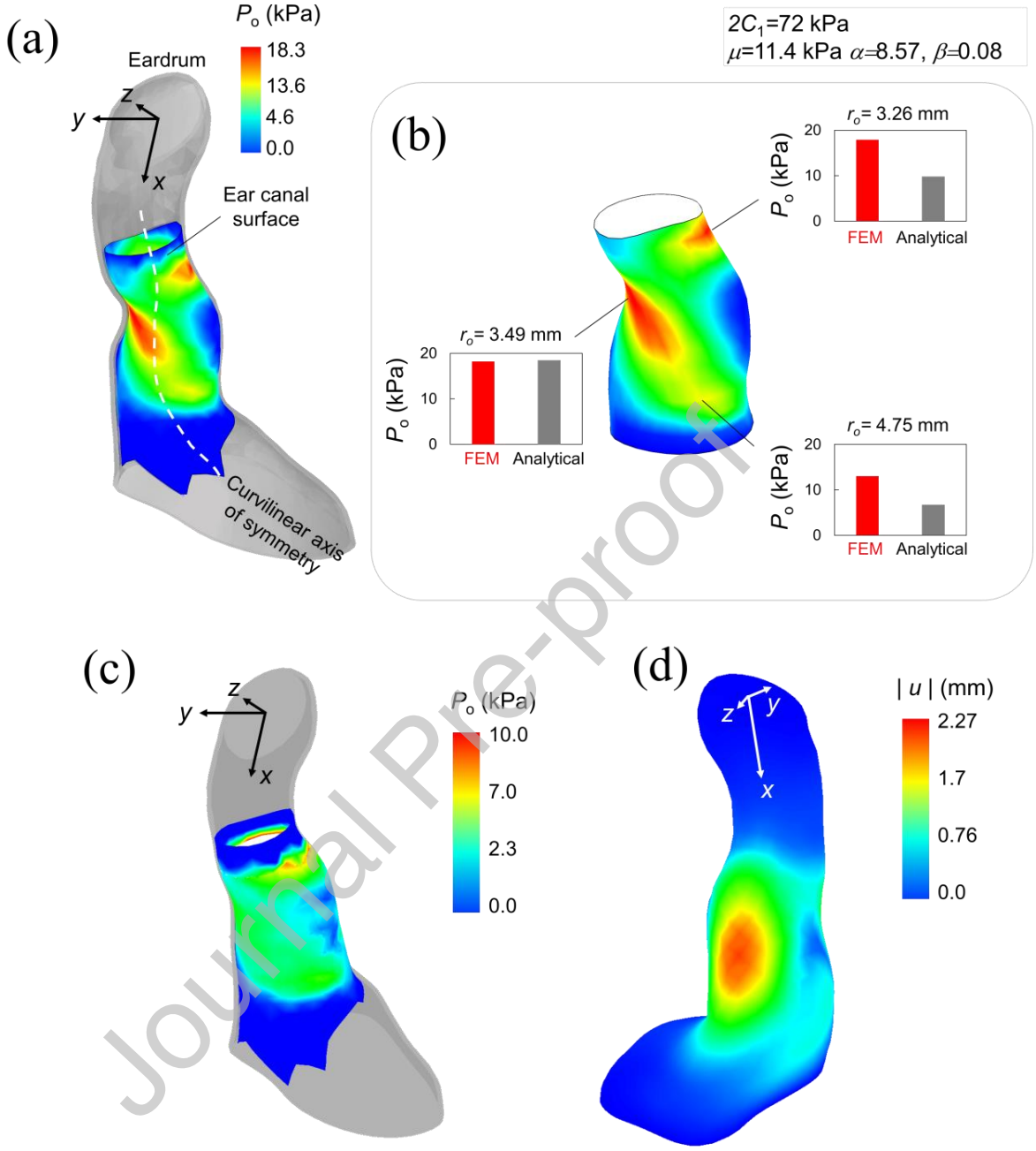

Figure 13: Pressure contour under rigid confinement at (a) earcanal surface and (b) highest pressure values and their comparison with analytical model estimates; (c) Pressure contour under unconfined conditions and its corresponding (d) displacement contour plot.

Since in reality, the cartilaginous part of the earcanal is surrounded by fatty and cartilage materials, we relaxed the boundary conditions at the outer surface of the earcanal by allowing those surrounding materials to deform freely (Supplementary materials 5, Figure S5b). This simulation serves as the other extreme where the earcanal is free to expand with the earplug, during which the dominant resistance is tensile forces from the thin skin layer. Figures 13c, d show the pressure contour developed on the interface surface of the earcanal along with its corresponding displacement field. The pressure roughly takes a similar spatial distribution as the previous case with a lower pressure range between 5-6 kPa. High stresses are developed at the sharp edge, which are ignored. In contrast to the previous case, the earcanal mostly takes the cylindrical shape of the earplug. Between the first and second bend, actual earcanal radius varies between 2.9−3.77 mm and the earplug (with radius a=6.5) is thus compressed in the range of 2−3.6 mm. Because of the absence of constraint on the outer surfaces of the skin layer, the earplug has therefore recovered more than 72% of its initial radius.

These two extreme cases indicate that the pressure limits are between 5 and 18.2 kPa. A previous study predicted a range of 10-60 kPa (discomforting earplugs) and 3-12 kPa (comfortable earplugs) [32]. In their work [32], they did not report their geometric dimensions of analyzed earcanal, which prevented one-to-one comparison. Additionally, they idealized the hyperelastic skin and earplug with linear elastic constitutive laws.

The threshold of comfort has not reached consensus [4]. Several works suggested that comfort is compromised when the pressure exceeds one of these limits: 9kPa [68], or 5kPa [69]. Clearly, these ranges are quite spread-out, based on those thresholds, our pressure calculation may tend to fall under the uncomfortable side (in terms of the physical comfort). The maximum pressure on Figure 13 was however localized between the first and second bend. While knowing that RD earplugs are among the least uncomfortable earplugs in terms of mechanical pressure, it may therefore be safe to speculate that the relative size of earcanal surface area that is engaged in contact affects the perception of comfort keeping in mind that other factors such as the sensitivity map of skin play also a role.

8. Conclusions

In this work, we developed several analytical and computational models to predict the pressure induced by rolled-down (RD) foam earplugs on the internal earcanal wall. We have started our analysis by considering a simplified cylindrical model of earcanal. We use finite element method to simulate the quasi-static radial compression of RD earplugs in this idealized earcanal and predict the resulting static mechanical pressure P_o induced on earcanal walls. The model adopted hyperelastic constitutive laws for earplugs and skin. We use this simplified model for examining the effect of the relative ratio of hyperelastic shear modulus of earplug (μ) to earcanal skin ($2C_1$): $\frac{\mu}{2C_1}$ on P_o and accordingly determine the applicability of assuming a rigid skin surface ($\frac{\mu}{2C_1}=0$). Assuming rigid earcanal skin allows the formulation of a simple analytical model that predicts the pressure P_o as a function of earplug and earcanal radius r_o, but excludes the skin properties.

We found that when the relative softness of earplug foam to earcanal skin ratio is $\frac{\mu}{2C_1}>7$, the properties of the skin becomes important because the earplug may induce nonneglibgible deformations. Otherwise, the rigid skin assumption which is applicable for a large range of $0<\frac{\mu}{2C_1}<7$, which leads to the analytical model of the form: $\frac{P_o(z)}{\mu}=-\frac{2}{\alpha}\left(\left(\frac{r_o(z)}{a}\right)^{\alpha-2}-\left(\frac{r_o(z)}{a}\right)^{-2\left(1+\frac{\alpha\beta}{1+\beta}\right)}\right)$, that can readily predict the pressure induced by earplugs for any axisymmetric earcanal profiles $r_o(z)$.

To achieve representative predictions using either computational or analytical models, we estimated the hyperelastic properties of the skin and RD-foam earplug using an inverse approach via simulations and experiments of forearm skin indentation and radial compression tests of earplugs. The characterization of skin properties reveals that we may simplify the skin as a single hyperelastic layer described by incompressible Neo-Hookean model with single parameter: $C_1=36$ kPa. For foam, we have utilized J-Crimp stent testing rig to calibrate the hyperelastic parameters of the RD-foam, which are: μ=11.4 kPa, α=8.57 and β=0.08. Those parameters where then used in the FE simulations of two other different experimental setups involving transverse

and uniaxial quasi-static compression. Comparisons between the simulation and experimental results show reasonable match between experiments and numerical results and thereby validate the proposed parameters along transverse direction and which indicate possible anisotropy in the mechanical response of the studied earplug.

Upon validation of RD-foam and skin properties, we develop two more realistic FE-models, namely; a curved axisymmetric model of earcanal and a 3D earcanal model of the earcanal skin. Both models have earcanal geometry that is reconstructed from actual MRI images of a healthy human participant. The axisymmetric model revealed that the pressure P_o is a function of earcanal radius $r(z)$ that varies along its axisymmetric z-axis with pressure range between 5-31 kPa. The 3D earcanal model revealed that the pressure on earcanal using RD-foam earplug range between 5-18.2 kPa depending on the hardness of the skin and tissue surrounding the earcanal.

Despite the insensitivity of the pressure P_o to properties of skin for the most part of the range between; $0 < \frac{\mu}{2C_1} < 7$, future work can consider a refinement of the properties of skin using indentation of earcanal skin experiments instead of a forearm, especially for stiffer earplugs. That is expected to lead to a more representative ratio $\frac{\mu}{2C_1}$ which excludes nonpresent materials near earcanal like the muscles tissue in forearms. Additionally, a realistic representation of the tissues surrounding the earcanal may be needed for simulating the full 3D earcanal model.

In addition, our assumption of minimal Poisson's effect for the earplug $\beta = 0.08$ is reasonable to capture the pressure induced by earplugs. However this value could be calibrated to better account for the kinematics of the earplugs and capture bulging effects which occur during the radial-Crimp compression and which are affected by friction between earplug and crimp teeth. Those RD-earplugs are sensitive to the amount of precompression, as we have observed qualitatively that with more compression the final static pressure gets lower. This behavior can be attributed to damage incurred during the precompression. Therefore, ad-hoc compression by hand may lead to variations across experimental tests. Systematic precompression via crimps may be employed in future works to exercise better control over the precompression process.

The maximum pressure prediction of the varying cross section area axisymmetric model (Figure 11) overestimates the pressure by a factor of 1.34 that of 3D earcanal model (Figure 13a).

This difference mainly emerges because axisymmetric condition is not applicable for actual earcanal geometry. These axisymmetric models can however still be used to compare different earplugs and to assess the effect of changing material and basic geometric parameters. One major advantage of those models is that they are handy and can be corrected to achieve representative values obtained from the computationally expensive 3D simulations or actual experiments. Finally, this work provides first steps in developing an objective physical comfort-index specific to earcanal.

This work have adopted a deterministic approach to finding the material parameters. However, it would be worth adopting Bayesian inferences (BI) accounting for the experimental variability in future works, where we identify systematically a range and distribution of the hyperelastic material parameters of the foam [70,71]. Besides, since our 3D simulations are computationally expensive, surrogate models based for example on neural networks could potentially provide a rapid modeling alternative [72,73]. In addition a goal oriented mesh refinement could be utilized for minimizing discretization error for a user-defined quantity [74].

Acknowledgements

This work was supported by MITACS [Grant Number IT10643] and IRSST [Grant Number 2015-0014].

Data availability

Data supporting the findings of this study are available from the corresponding authors upon reasonable request.

Declaration of interests

☒ The authors declare that they have no known competing financial interests or personal relationships that could have appeared to influence the work reported in this paper.

CRediT authorship contribution statement

Ahmed S. Dalaq: Conceptualization, Formal Analysis, Methodology, Software, Writing − Original draft, Visualization. **Luiz G. C. Melo**: Investigation, Formal Analysis, Writing – review and editing, Data curation. **Franck Sgard**: Methodology, Writing – review and editing, Supervision, Funding acquisition. **Olivier Doutres**: Project administration, Resources, Writing – review and editing, Supervision, Funding acquisition. **Eric Wagnac:** Writing – review and editing, Supervision.

10. References

[1] T.J. Ryan, R.S. Meier, A. Tatarka, Improved hearing protector attenuation through the use of a lubricant, Journal of Occupational and Environmental Hygiene. 14 (2017) 931–937. https://doi.org/10.1080/15459624.2017.1358815.
[2] S. Yongbing, W. Hal Martin, Noise Induced Hearing Loss in China: A Potentially Costly Public Health Lssue, Journal of Otology. 8 (2013) 51–56. https://doi.org/10.1016/S1672-2930(13)50007-9.
[3] O. Doutres, F. Sgard, J. Terroir, N. Perrin, C. Jolly, C. Gauvin, A. Negrini, A critical review of the literature on comfort of hearing protection devices: Analysis of the comfort measurement variability, International Journal of Occupational Safety and Ergonomics. (2020) 1–36. https://doi.org/10.1080/10803548.2020.1772546.
[4] O. Doutres, F. Sgard, J. Terroir, N. Perrin, C. Jolly, C. Gauvin, A. Negrini, A critical review of the literature on comfort of hearing protection devices: definition of comfort and identification of its main attributes for earplug types, International Journal of Audiology. 58 (2019) 12.
[5] M.-Y. Park, J.G. Casali, An empirical study of comfort afforded by various hearing protection devices: Laboratory versus field results, Applied Acoustics. 34 (1991) 151—179. https://doi.org/10.1016/0003-682X(91)90082-P.
[6] R. Zemp, W.R. Taylor, S. Lorenzetti, Are pressure measurements effective in the assessment of office chair comfort/discomfort? A review, Applied Ergonomics. 48 (2015) 273–282. https://doi.org/10.1016/j.apergo.2014.12.010.
[7] S.K. Bhattacharya, S.R. Tripathi, S.K. Kashyai, Assessment of comfort of various hearing protection devices (HPD)., Journal of Human Ergology. 22 (1993) 163–172.
[8] L.F.M. Kuijt-Evers, T. Bosch, M.A. Huysmans, M.P. de Looze, P. Vink, Association between objective and subjective measurements of comfort and discomfort in hand tools, Applied Ergonomics. 38 (2007) 643–654. https://doi.org/10.1016/j.apergo.2006.05.004.
[9] A. Bockstael, L. De Bruyne, B.B. Vinck, Attitudes and beliefs concerning hearing protectors and noise exposure, Canadian Acoustics. 39 (2011) 92–93.
[10] P.M. Arezes, J.S. Baptista, M.P. Barroso, P. Carneiro, P. Cordeiro, N. Costa, R.B. Melo, S. Miguel, G. Perestrelo, International Symposium on Occupational Safety and Hygiene, Occupational safety and hygiene, CRC Press, Boca Raton, Fla, 2013.
[11] T.C. Morata, A.C. Fiorini, F.M. Fischer, E.F. Krieg, L. Gozzoli, S. Colacioppo, others, Factors affecting the use of hearing protectors in a population of printing workers, Noise and Health. 4 (2001) 25.
[12] P. Arezes, C. Abelenda, A.C. Braga, An evaluation of comfort afforded by hearing protection devices, (2008). http://repositorium.sdum.uminho.pt/handle/1822/19304 (accessed June 28, 2016).
[13] P.M. Arezes, A.S. Miguel, Assessing the use of hearing protection in industrial settings: A comparison between methods, International Journal of Industrial Ergonomics. 43 (2013) 518–525. https://doi.org/10.1016/j.ergon.2012.07.002.
[14] R.R. Davis, W.J. Murphy, D.C. Byrne, P.B. Shaw, Acceptance of a semi-custom hearing protector by manufacturing workers, Journal of Occupational and Environmental Hygiene. 8 (2011) D125–D130. https://doi.org/10.1080/15459624.2011.626262.
[15] D.L. Ronis, O. Hong, S.L. Lusk, Comparison of the original and revised structures of the health promotion model in predicting construction workers' use of hearing protection, Research in Nursing & Health. 29 (2006) 3–17. https://doi.org/10.1002/nur.20111.
[16] O. Hong, D.L. Chin, D.L. Ronis, Predictors of Hearing Protection Behavior Among Firefighters in the United States, International Journal of Behavioral Medicine. 20 (2013) 121–130. https://doi.org/10.1007/s12529-011-9207-0.
[17] M.-A. Gaudreau, F. Sgard, F. Laville, H. Nélisse, A finite element model to improve noise reduction based attenuation measurement of earmuffs in a directional sound field, Applied Acoustics. 119 (2017) 66–77. https://doi.org/10.1016/j.apacoust.2016.12.003.
[18] G. Viallet, F. Sgard, F. Laville, J. Boutin, A finite element model to predict the sound attenuation of earplugs in an acoustical test fixture, The Journal of the Acoustical Society of America. 136 (2014) 1269–1280. http://dx.doi.org/10.1121/1.4890645.

[19] M. Brummund, F. Sgard, Y. Petit, F. Laville, On the influence of the material properties of the external ear on occlusion effect simulations, in: Canadian Acoustics, Banff, AB, Canada, 2012: pp. 110–111.
[20] F. Sgard, M. Brummund, G. Viallet, S. Boyer, O. Doutres, Y. Petit, H. Nélisse, F. Laville, J. Boutin, Prediction of airborne and structure borne sound transmission through hearing protectors using FEM, in: Proceedings of Internoise 2014, Melbourne, Australia, 2014.
[21] A. Damongeot, R. Lataye, A. Kusy, An empirical formula for predicting the attenuation given by double hearing protection (earplugs and earmuffs), Applied Acoustics. 28 (1989) 169—175. https://doi.org/10.1016/0003-682X(89)90091-1.
[22] J.B. Tufts, S. Chen, L. Marshall, Attenuation as a function of the canal length of custom-molded earplugs: A pilot study, The Journal of the Acoustical Society of America. 133 (2013) EL446–EL451. https://doi.org/10.1121/1.4802896.
[23] B.W. Epps, J.G. Casali, Hearing Protection Device Comfort and User Preference: An Investigation and Evaluation Methodology, in: Proceedings of the Human Factors and Ergonomics Society Annual Meeting, SAGE Publications, 1985: pp. 814–818. http://pro.sagepub.com/content/29/8/814.short (accessed June 28, 2016).
[24] J.G. Casali, S.T. Lam, B.W. Epps, Rating and ranking methods for hearing protector wearability, Sound and Vibration. 21 (1987) 10–18.
[25] K.F. Sweetland, Physical predictors for earmuff comfort, Master's thesis, Loughborough University, 1983. https://dspace.lboro.ac.uk/dspace-jspui/handle/2134/12214 (accessed July 4, 2016).
[26] Anonymous, ISO standard, "Moderate thermal environments – Determination of the PMV and PPD indices and specification of the conditions for thermal comfort", ISO 7730, (1994).
[27] J.F. Knight, C. Baber, A tool to assess the comfort of wearable computers, Hum Factors. 47 (2005) 77–91.
[28] M.P. de Looze, L.F.M. Kuijt-Evers, J. van Dieën, Sitting comfort and discomfort and the relationships with objective measures, Ergonomics. 46 (2003) 985–997. https://doi.org/10.1080/0014013031000121977.
[29] B.A. Crane, M.B. Holm, D. Hobson, R.A. Cooper, M.P. Reed, Responsiveness of the TAWC tool for assessing wheelchair discomfort, Disabil Rehabil Assist Technol. 2 (2007) 97–103.
[30] S.N.Y. Gerges, Earmuff comfort, Applied Acoustics. 73 (2012) 1003–1012. https://doi.org/10.1016/j.apacoust.2012.04.015.
[31] R.R. Davis, others, What do we know about hearing protector comfort?, Noise and Health. 10 (2008) 83.
[32] A.T. Baker, S. Lee, F. Mayfield, Evaluating Hearing Protection Comfort Through Computer Modeling, in: Simulia Customer Conference, 2010: p. 15. http://www.simulia.com/forms/world/pdf2010/Baker_SCC2010.pdf.
[33] J. Norris, R. Chambers, N. Kattamis, B. Davis, J. Bieszczad, Effects of custom earplug design parameters on achieved attenuation, in: Poster Presentation at the Annual Meeting of the National Hearing Conservation Association, New Orleans, LA, 2011. http://www.hearingconservation.org/associations/10915/files/2012NHCAPosterCustomMoldedDesignlowres.pdf (accessed June 27, 2016).
[34] C.R. Smith, R.M.J. Broughton, J.N. Wilmoth, T.E. Borton, Physical characteristics and attenuation of foam earplugs, Am. Ind. Hyg. Assoc. J. 43 (1982) 31–38.
[35] A.R. Graydon, B. Stoddart, K.G. Blyth, G.F. Brunner, Comfortable foam-based ear plugs, EP 1 192 920 A1, 2002. http://www.google.com/patents/EP1192920A1 (accessed July 5, 2016).
[36] E.H. Berger, Dynamic and Static Material Properties of E.A.R Plug foam, (1998).
[37] L. Qi, H. Liu, J. Lutfy, W.R.J. Funnell, S.J. Daniel, A nonlinear finite-element model of the newborn ear canal, Journal of the Acoustical Society of America. 120 (2006) 3789–3798.
[38] S. Benacchio, . Doutres, A. Varoquaux, E. Wagnac, A. Le Troter, V. Callot, F. Sgard, Use of magnetic resonance image registration to estimate displacement in the human earcanal due to the insertion of in-ear devices, The Journal of the Acoustical Society of America. 146 (2019) 2452–2465. https://doi.org/10.1121/1.5126857.

[39] V. Tran, F. Charleux, M. Rachik, A. Ehrlacher, M.C. Hobatho, In vivo characterization of the mechanical properties of human skin derived from MRI and indentation techniques, Journal of Biomechanics. 41 (2007) S29. https://doi.org/10.1016/S0021-9290(08)70029-0.
[40] B. Storåkers, On material representation and constitutive branching in finite compressible elasticity, Journal of the Mechanics and Physics of Solids. 34 (1986) 125–145. https://doi.org/10.1016/0022-5096(86)90033-5.
[41] H. Jin, J.L. Lewis, Determination of Poisson's ratio of articular cartilage by indentation using different-sized indenters, J Biomech Eng. 126 (2004) 138–145. https://doi.org/10.1115/1.1688772.
[42] M.F. Griffin, Y. Premakumar, A.M. Seifalian, M. Szarko, P.E.M. Butler, Biomechanical Characterisation of the Human Auricular Cartilages; Implications for Tissue Engineering, Ann Biomed Eng. 44 (2016) 3460–3467. https://doi.org/10.1007/s10439-016-1688-1.
[43] R. Hill, A general theory of uniqueness and stability in elastic-plastic solids, Journal of the Mechanics and Physics of Solids. 6 (1958) 236–249. https://doi.org/10.1016/0022-5096(58)90029-2.
[44] 3M™ E-A-R™ Classic™ Earplugs 312-1082, Uncorded, Econopack Dispenser Box, 3000 Pair/Case, (n.d.). https://www.3m.com/3M/en_US/company-us/all-3m-products/~/3M-E-A-R-Classic-Earplugs-312-1082-Uncorded-Econopack-Dispenser-Box-3000-Pair-Case/?N=5002385+3294780166&rt=rud (accessed February 15, 2021).
[45] D.C. Drucker, A definition of a stable inelastic material, Journal of Applied Mechanics. 26 (1959) 101–195.
[46] M.L. Ju, S. Mezghani, H. Jmal, R. Dupuis, E. Aubry, Parameter Estimation of a Hyperelastic Constitutive Model for the Description of Polyurethane Foam in Large Deformation, Cellular Polymers. 32 (2013) 21–40. https://doi.org/10.1177/026248931303200102.
[47] S. Kim, H. Shin, S. Rhim, K.Y. Rhee, Calibration of hyperelastic and hyperfoam constitutive models for an indentation event of rigid polyurethane foam, Composites Part B: Engineering. 163 (2019) 297–302. https://doi.org/10.1016/j.compositesb.2018.11.045.
[48] M. Schrodt, G. Benderoth, A. Kühhorn, Hyperelastic Description of Polymer Soft Foams at Finite Deformations, Undefined. (2005). /paper/Hyperelastic-Description-of-Polymer-Soft-Foams-at-Schrodt-Benderoth/4095aa398c8e2d30696e4fbdbba4de054f4a6104 (accessed April 25, 2021).
[49] Blockwise, Model TTR2, Blockwise Engineering. (n.d.). http://blockwise.com/radial-force-testers/ttr2/ (accessed February 15, 2021).
[50] J.C. Lagarias, J.A. Reeds, M.H. Wright, P.E. Wright, Convergence Properties of the Nelder--Mead Simplex Method in Low Dimensions, SIAM J. Optim. 9 (1998) 112–147. https://doi.org/10.1137/S1052623496303470.
[51] S. Benacchio, O. Doutres, A. Le Troter, A. Varoquaux, E. Wagnac, V. Callot, F. Sgard, Estimation of the ear canal displacement field due to in-ear device insertion using a registration method on a human-like artificial ear, Hearing Research. 365 (2018) 16–27. https://doi.org/10.1016/j.heares.2018.05.019.
[52] J.-F. Yu, K.-C. Lee, R.-H. Wang, Y.-S. Chen, C.-C. Fan, Y.-C. Peng, T.-H. Tu, C.-I. Chen, K.-Y. Lin, Anthropometry of external auditory canal by non-contactable measurement, Applied Ergonomics. 50 (2015) 50–55. https://doi.org/10.1016/j.apergo.2015.01.008.
[53] B. Ballachanda, The Human Ear Canal, Plural Publishing, 2013.
[54] Simulia, Abaqus/CAE User's Guide 6.14, (2014).
[55] E.J. Bos, M. Pluemeekers, M. Helder, N. Kuzmin, K. van der Laan, M.-L. Groot, G. van Osch, P. van Zuijlen, Structural and Mechanical Comparison of Human Ear, Alar, and Septal Cartilage, Plast Reconstr Surg Glob Open. 6 (2018). https://doi.org/10.1097/GOX.0000000000001610.
[56] D.T. Reilly, A.H. Burstein, V.H. Frankel, The elastic modulus for bone, Journal of Biomechanics. 7 (1974) 271–275. https://doi.org/10.1016/0021-9290(74)90018-9.
[57] A.P. Zeltwanger, J. Wang, G. Bertocci, D. Brienza, V.S. Chib, Effective Young's modulus of buttocks soft tissue, in: ERIC, 2000: p. 375.

[58] K. Senol, A. Shukla, Dynamic response of closed cell PVC foams subjected to underwater shock loading, International Journal of Impact Engineering. 130 (2019) 214–225. https://doi.org/10.1016/j.ijimpeng.2019.04.020.
[59] V. Tita, M.F. Caliri Júnior, R.A. Angélico, R.B. Canto, Experimental analyses of the poly(vinyl chloride) foams' mechanical anisotropic behavior, Polymer Engineering & Science. 52 (2012) 2654–2663. https://doi.org/10.1002/pen.23222.
[60] K.L. Johnson, Contact Mechanics, Cambridge University Press, Cambridge, 1985. https://doi.org/10.1017/CBO9781139171731.
[61] A.C. Ugural, S.K. Fenster, Advanced Mechanics of Materials and Applied Elasticity, Pearson Education, 2011.
[62] Blockwise, Measuring Radial Force, (2000). https://blockwise.com/wp-content/uploads/2020/08/K050-Measuring-Radial-Force.pdf (accessed January 13, 2022).
[63] Blockwise, Hoop Force - Radial Force - Pressure Derivation, (2000). https://blockwise.com/wp-content/uploads/2020/08/R862-HoopForce-RadialForce-Pressure-Derivation.pdf (accessed May 2, 2022).
[64] E.H. Berger, Tips & Tools for Fitting and using E-A-R Foam Earplugs, (n.d.) 16.
[65] R. Maiti, M. Duan, S.G. Danby, R. Lewis, S.J. Matcher, M.J. Carré, Morphological parametric mapping of 21 skin sites throughout the body using optical coherence tomography, Journal of the Mechanical Behavior of Biomedical Materials. 102 (2020) 103501. https://doi.org/10.1016/j.jmbbm.2019.103501.
[66] R.M. Hackett, Hyperelasticity Primer, Springer International Publishing, 2016. https://doi.org/10.1007/978-3-319-23273-7.
[67] COMSOL: Multiphysics Software for Optimizing Designs, COMSOL. (n.d.). https://www.comsol.com/ (accessed April 29, 2021).
[68] A.R. Graydon, K.G. Blyth, B. Stoddart, G.F. Brunner, COMFORTABLE FOAM-BASED EAR PLUGS FOR EFFECTIVE SOUND ATTENUATION, WO2002026177A1, 2002.
[69] W.J. Staab, W. Sjursen, D. Preves, T. Squeglia, A one-size disposable hearing aid is introduced, The Hearing Journal. 53 (2000) 36. https://doi.org/10.1097/00025572-200004000-00004.
[70] H. Rappel, L.A.A. Beex, J.S. Hale, L. Noels, S.P.A. Bordas, A Tutorial on Bayesian Inference to Identify Material Parameters in Solid Mechanics, Arch Computat Methods Eng. 27 (2020) 361–385. https://doi.org/10.1007/s11831-018-09311-x.
[71] A. Elouneg, D. Sutula, J. Chambert, A. Lejeune, S.P.A. Bordas, E. Jacquet, An open-source FEniCS-based framework for hyperelastic parameter estimation from noisy full-field data: Application to heterogeneous soft tissues, Computers & Structures. 255 (2021) 106620. https://doi.org/10.1016/j.compstruc.2021.106620.
[72] S. Deshpande, J. Lengiewicz, S.P.A. Bordas, Probabilistic Deep Learning for Real-Time Large Deformation Simulations, Computer Methods in Applied Mechanics and Engineering. 398 (2022) 115307. https://doi.org/10.1016/j.cma.2022.115307.
[73] H.P. Bui, S. Tomar, H. Courtecuisse, S. Cotin, S.P.A. Bordas, Real-Time Error Control for Surgical Simulation, IEEE Transactions on Biomedical Engineering. 65 (2018) 596–607. https://doi.org/10.1109/TBME.2017.2695587.
[74] M. Duprez, S.P.A. Bordas, M. Bucki, H.P. Bui, F. Chouly, V. Lleras, C. Lobos, A. Lozinski, P.-Y. Rohan, S. Tomar, Quantifying discretization errors for soft tissue simulation in computer assisted surgery: A preliminary study, Applied Mathematical Modelling. 77 (2020) 709–723. https://doi.org/10.1016/j.apm.2019.07.055.

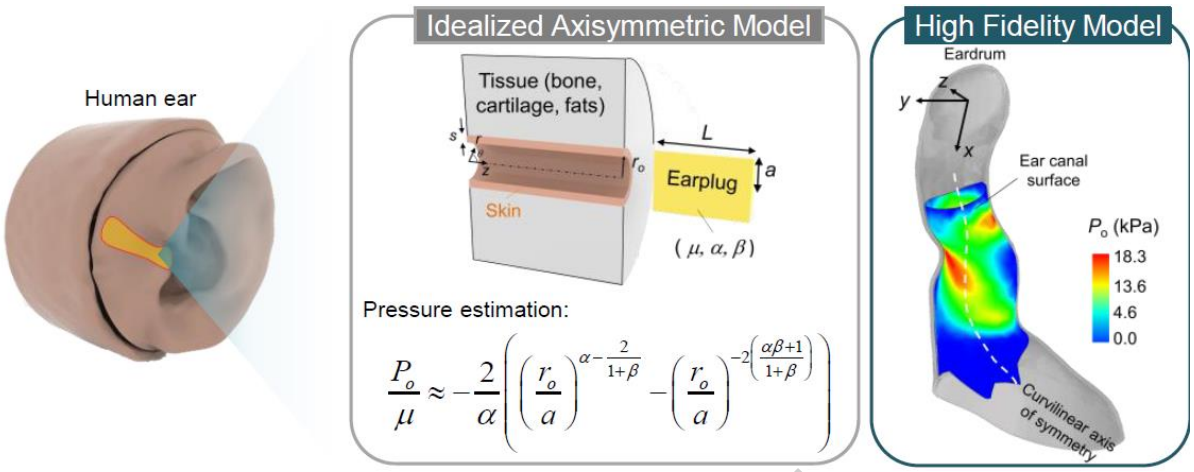

Graphical Abstract